UPPSALA UNIVERSITY
Department of Radiation Sciences
Box 535, S-751 21 Uppsala, Sweden
http://www.tsl.uu.se/

Internal report

ISV-4/97

February 1996

Determination of the residual thermal power in spent nuclear fuel from gamma-ray measurements

Peter Jansson*

Dept. of Radiation Sciences, Uppsala University, Box 535, S-751 21 Uppsala, Sweden

Abstract: A method of determining the decay heat in spent nuclear fuel using the gamma radiation from ^{137}Cs is presented. The method is useful for fuel assemblies with a cooling time longer than 5 years.

Experimental tests of the method are presented for eleven 8x8 BWR fuel assemblies with cooling times in the range 5 to 15 years. The decay heat is determined with a 3.5 % error for these assemblies. Simulations with the code Origen2.1 shows that this uncertainty can be expected to be reduced for fuel assemblies with cooling times of the order of 40 years.

* peter.jansson@tsl.uu.se

Determination of the Residual Thermal Power in Spent Nuclear Fuel from Gamma-Ray Measurements

Peter Jansson

Thesis for the degree of Master of Science

Uppsala University

1996-02-01

Table of Contents

1 Introduction

At present, Sweden has twelve nuclear power plants. About half of the electric power in Sweden is produced in these plants. If all nuclear reactors are used until the year 2010, they will produce about 200000 m^3 waste, ref. [16]. This amounts to about 8000 tonnes of spent nuclear fuel, ref [17], that need to be taken care of.

In Sweden, there is an understanding between scientist, authorities and government that the nuclear waste should be buried deep within the bed-rock of Sweden, in a final repository. There will be several protective barriers between the spent nuclear fuel and the surroundings, since the waste is hazardous and has to be encapsulated for many thousands of years.

The fuel itself is the first barrier. It is composed of uranium dioxide, a ceramic compound that is very difficult to solve in water. The fuel is planned to be encapsulated in a canister made of copper that protects the fuel from corroding. Even though there is little or no oxygen in the water at these depths, there are small amounts of other substances that give rise to a very slow corroding process of the copper canister.

Around the canister there will be bentonite clay filling up the space between the canisters and the surrounding rocks. This clay expands if it is in contact with water, therefore it hinders movement of water. It is also protective against small dislocations of the rocks.

Finally, the bed-rock around the storage facility provides a chemical and mechanically stable environment.

The spent nuclear fuel canisters are made so that they will remain sealed during a long period of time. They must not corrode in the water that may be present in the surrounding rocks, nor must they break apart due to possible mechanical stresses.

To achieve these goals, they are proposed to be made of an internal container of stainless steel, for the mechanical stability, and an outer layer of copper, that provides the corrosion protection. Studies show that the canister probably will remain sealed during millions of years ahead, which is more than enough for Sweden's spent nuclear fuel.

The temperature of the bentonite clay closest to the canister must be limited to 90° C or less. This limits the maximum surface thermal power dissipated by the spent nuclear fuel canister, but it also limits the size of the canister, and the decay heat in the nuclear fuel. At present there is a reference canister chosen containing 12 BWR assemblies or 4 PWR assemblies. This canister is limited to contain a maximum power of decay heat of about 1400 W. This means that it is interesting to device a method that can determine the decay heat in the spent nuclear fuel in a fast, accurate and reliable way.

In an earlier report, /ref. [1]/, a method of determining the decay heat experimentally was presented. It fulfils the demands of the final repository of a short measuring time. Furthermore, the method can be combined with the measurement of cooling time and burn-up of the spent nuclear fuel for safeguard purposes. The method uses the gamma radiation from fission products in the spent nuclear fuel for passive measurements of the average intensities from different isotopes, mainly ^{137}Cs, to determine the decay heat. The data are calibrated on calorimetric measurements of the decay heat.

This report, which forms a thesis for the degree of M.Sc., presents an experimental investigation of the usefulness of the method. It is based on measurements on eleven BWR fuel assemblies. These assemblies have been measured by gamma scanning and the results have been combined with results of calorimetric measurements. Calculations with Origen2.1 have been performed in order to investigate the sensitivity of the results to various fuel parameters. The calorimetric method has been improved by theoretical calculations and experiments regarding the escape of gamma radiation from the calorimeter.

2 Description of the Method

The emphasis in this thesis is put on an experimental study of a method to determine the decay power in spent fuel assemblies using gamma radiation from fission products. The method requires a direct comparison curve between intensity and decay heat, which can serve as a calibration. In the planned encapsulation plant this calibration curve can be used for obtaining the decay heat from an experimental measurement of the gamma radiation from fission products. This chapter concerns the establishment of such a calibration curve. A theoretical study is first presented where simulations with the Origen2.1 code was made. Then an experimental establishment of a calibration curve is presented using eleven fuel assemblies.

The assemblies studied in this work had cooling times from 4 to 15 years. The operator declared data regarding cooling time, initial enrichment and burn-up for these assemblies are shown in table 1.

Assembly number	Cooling time [d]	Initial enrich -ment [%]	<Burnup> [Mwd/tU]
8327	1496	2.903	37842.16
8332	2595	2.895	34974.48
8338	2595	2.911	34823.08
1136	4473	2.491	22236.00
582	5552	2.255	21268.00
596	5552	2.255	22256.00
710	4803	2.258	22608.00
900	4803	2.258	23160.00
6423	2595	2.900	35105.52
6432	2595	2.894	36853.96
6454	3317	2.898	37234.64

Table 1. Summary of operator declared data of the fuel assemblies studied in this work.

2.1 Gamma Emitting Nuclides

The encapsulation of the fuel is planned to take place after a cooling time of at least two decades. After such a long cooling time almost all gamma activity arises from the decay of the isotopes ^{137}Cs, ^{134}Cs and ^{154}Eu, see e.g. chapter 1.2 of reference [2].

^{137}Cs

The activity of ^{137}Cs is proportional to the burnup of the fuel and this activity is relatively insensitive to the enrichment of the fuel, /ref. [3]/. The total gamma radiation contributes to the decay heat by an almost constant fraction, see chapter 3. Since almost all of the gamma activity arises from the decay of ^{137}Cs at the cooling times of interest here, it is a reasonably good approximation that the ^{137}Cs intensity depends linearly on decay heat.

^{134}Cs

The relation between the ^{134}Cs activity and burnup is more complicated than the ^{137}Cs case since ^{134}Cs is produced mainly in the neutron capture process in ^{133}Cs. The relationship between the total decay heat and the gamma intensity from ^{134}Cs is accordingly more complicated than for ^{137}Cs. Furthermore, the half-life of ^{134}Cs is 2.1 years, which means that the ^{134}Cs fraction of the decay heat has become insignificant by the time the fuel assemblies are to be encapsulated. The possible use of ^{134}Cs as a measure of the decay heat is thus restricted to assemblies with cooling times below 20 years.

^{154}Eu

^{154}Eu is an isotope that is produced via many different mass chains, of which five contribute significantly. Therefore, it is difficult to make a simple mathematical treatment of the production of this isotope.

The use of ^{154}Eu is limited by it's half-life of 8.6 years. It might be possible to use this isotope in the determination of the decay heat for those assemblies which do not have an extremely long cooling time, i.e. exceeding about 50 years.

^{137}Cs+^{134}Cs+^{154}Eu

Origen2.1 simulations, (section 3), show that the relative contribution to decay heat from this sum is relatively constant in time for the assemblies studied here. This can be understood by the following discussion: At short cooling times the contribution from ^{134}Cs and other short-lived isotopes is dominant, while at long cooling times the contribution is mainly from ^{137}Cs. This implies that the sum of these isotopes is more constant in time than the contribution from individual isotopes, especially at short cooling times.

2.2 The Relation Between the Decay Heat and the Gamma-Ray Intensity

It was shown in reference [1] that the decay heat P of a fuel assembly after a cooling time of > 5-10 years can be expected to be nearly linearly dependent on the ^{137}Cs activity.

If the average radiation intensity I of the latter is measured in a gamma-scanning experiment one may write

$$P = \text{Const.} \cdot I \qquad \textit{Eq 1}$$

Only a fraction f of P is due to the ^{137}Cs + ^{137}Ba activity. We may thus rewrite P as

$$P = \frac{C}{f} \cdot I \qquad \textit{Eq 2}$$

where the proportionality constant C (unit: [Watts] / [counts per second]) depends on the geometry of the gamma-scanning experiment and on the type of fuel assembly.

The constant C must be determined in a calibration procedure. In this the ^{137}Cs-intensity I is determined for a number of calibration assemblies with known values of the fuel parameters. The calibration assemblies should preferably show large variations in these parameters. The decay heat of each calibration assembly is measured in a calorimetric measurement.

The factor f is essentially a constant, i.e. it depends only weakly on the type of fuel and its parameters burn-up (BU), cooling time (CT) and initial enrichment (ε), see figure 1 to figure 3.

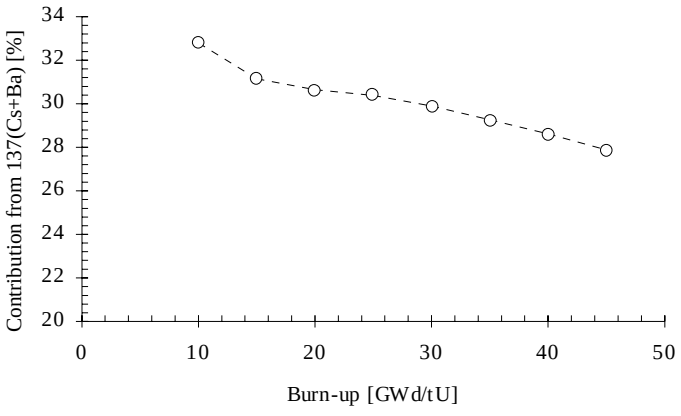

Figure 1. Contribution from ^{137}Cs+^{137}Ba to total decay heat as a function of burn-up for CT=40 years. The initial enrichment was ε = 2 % and the number of power cycles was 5. From ref. [1].

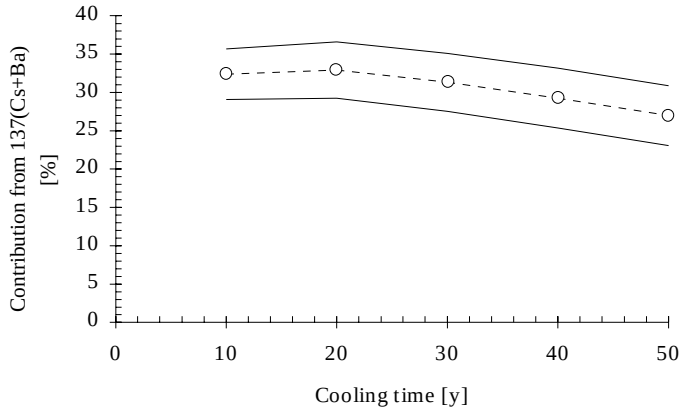

Figure 2. Contribution from $^{137}Cs+^{137}Ba$ to total decay heat as a function of cooling time at burn-up = 35 GWd/tU. The initial enrichment was ε = 2 % and the number of power cycles was 5. The solid lines represent the estimated uncertainty. From ref. [1].

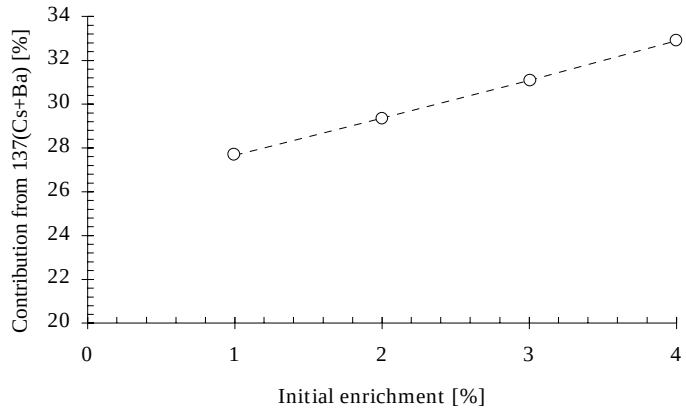

Figure 3. Contribution from $^{137}Cs+^{137}Ba$ to decay heat as a function of initial enrichment. The calculations were performed with 5 power cycles and the burn-up and cooling time were 35 GWd/tU and 40 years. From ref. [1].

If the time t_1 when the gamma-scanning is made and the time t_2 when the calorimetric measurement was made are significantly different, the measured gamma intensity for each calibration assembly must be corrected for the time elapsed between these measurements.

eq 2 then becomes

$$P = \frac{C}{f} \cdot I \cdot e^{-\lambda \cdot t} \qquad \textit{Eq 3}$$

where λ is the decay constant of ^{137}Cs and $t = t_2 - t_1$.

In practice the experimental geometry can be assumed to be constant, but the value of C in principle has to be determined for each type of fuel assembly. The variation in C between different types of assemblies is

however not expected to be very large, since the outer dimensions are the same for all assemblies and no large variation is expected in the fuel to moderator ratio.

When eq 3 is applied for determining the decay heat P from the measured intensity I, the factor f must be known for each assembly. However, as observed above, only small variations are expected in the value of f. For a majority of the assemblies, which can be expected to have fuel parameters within the range indicated in table 2, the value of f is expected to vary less than 5 %.

Fuel parameter	Typical value and deviation	Δf / f
BU [GWd / t]	35 ± 5	± 2.6 %
CT [y]	30 ± 5	± 2.8 %
ε [%]	2.5 ± 0.5	± 2.6 %

Table 2. Variations in the factor f with three important fuel parameters. f is calculated with Origen2.1.

Provided that such an accuracy in the determination of the decay heat is satisfactory, a constant standard value of f could be used in eq 3. If a higher accuracy of f is needed, or the fuel parameters are out of their normal range, the standard value must be corrected. Since this correction normally is small, one may suggest that it need not be calculated with a full Origen2.1 calculation for the specific case. Instead sufficiently accurate corrections should be obtainable from simple tables based on Origen calculations for near-standard cases, cf. figure 1 to figure 3.

3 Simulations

In this report experimental measurements are presented for eleven of the fuel assemblies at CLAB[†]. These fuel assemblies have been calorimetrically measured (regarding the decay heat) by staff at CLAB as well as gamma scanned. Here we describe Origen2.1 simulations performed using the operator declared power histories of these fuel assemblies in order to simulate the experimental results and to calculate the gamma-fraction f as discussed in section 2.2.

The fuel parameters for the fuel assemblies are given in table 1. In the calculations these parameters were kept fixed except for the cooling time, which was the only parameter varied. The output files from these calculations contain the radioactivity and decay heat from various isotopes, including ^{134}Cs, ^{137}Cs, ^{137}Ba and ^{154}Eu. The results of these simulations are tabulated in appendix 6.6.

The intensity from different isotopes and the decay heat should be correlated as discussed in sections 2.1 and 2.2. Therefore the output from the simulations is first directed towards these dependencies.

figure 4 and figure 5 show the calculated relations between intensities and decay heat for the fuel assemblies of table 1. In figure 4 the cooling time has been set to the time when the calorimetric measurement was performed. figure 5 shows the corresponding calculation when the cooling time of all assemblies has been adjusted to a typically long time, here taken as 37 years. For the shorter cooling times (in the range of 4 - 15 years) the relation for ^{137}Cs is seen to be rather non-linear, while it is nearly linear for the summed gamma intensities. For the long cooling-time the relation is very nearly linear with a standard deviation of less than 3 %. The points show a slight systematic effect relative to the line. This effect has been observed in ref. [1] and is due to the fact that processes other than the ^{137}Cs + ^{137}Ba decay, especially the actinides, contribute to the total decay heat.

[†] CLAB='Centralt mellanlager för använt bränsle'.

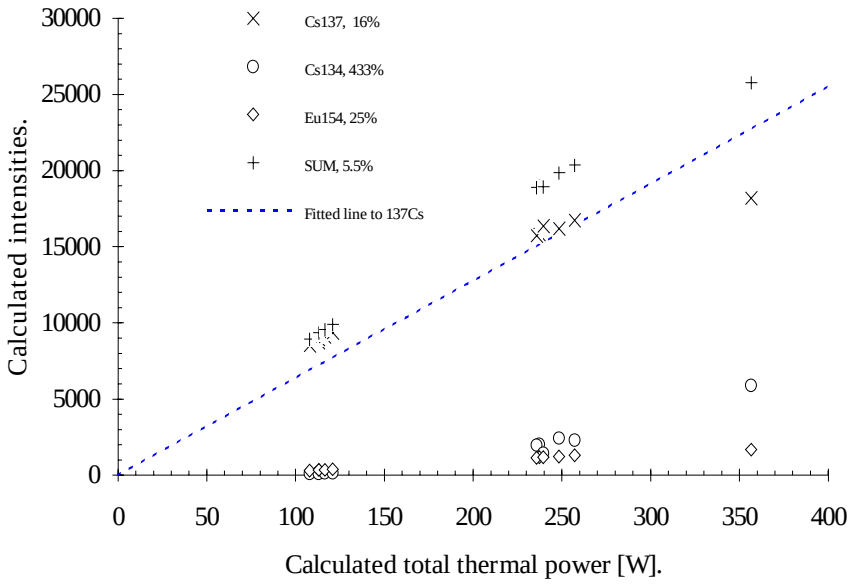

Figure 4. Calculated intensity versus calculated total decay heat. The cooling time used here is the time difference between the calorimetric measurement and the out of core date. The numbers in the legend show the relative standard deviation of the points to a straight line through origin.

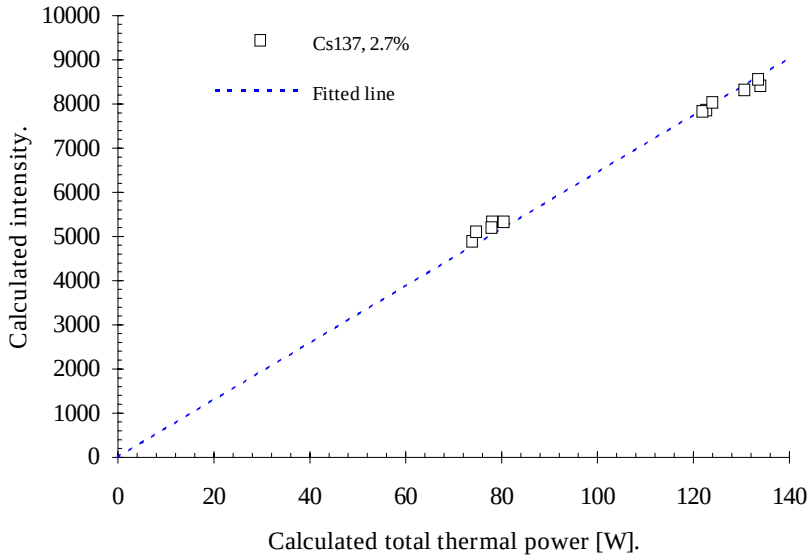

Figure 5. Calculated intensity from ^{137}Cs versus calculated total decay heat at a cooling time of 37 years for the assemblies studied in this work.

Linearisation of the Measured Intensities

The dependence of the intensities as a function of the decay heat shows a non-linear behaviour at the short cooling times of the fuel assemblies studied in this work. This means that the calibration would be non-linear at short cooling times and it is difficult to know the form of the functional dependence, which also depends somewhat on burn-up and enrichment. In order to facilitate calibrations and comparisons it is desirable to correct the measured intensities relative to the decay heat in order to achieve an easily applicable linear functional dependence as discussed in section 2.2. This linearisation procedure should be used also for fuel assemblies with large cooling times in order to improve on the linear dependence. Therefore, Origen2.1 was used to calculate the gamma-fraction, f, of the decay heat. figure 6 shows the gamma-fraction, f, for the isotopes of interest and the fuel assemblies investigated at the time of the calorimetric measurement. One may note the regular behaviour of the summed intensities in comparison to the intensities from the individual isotopes.

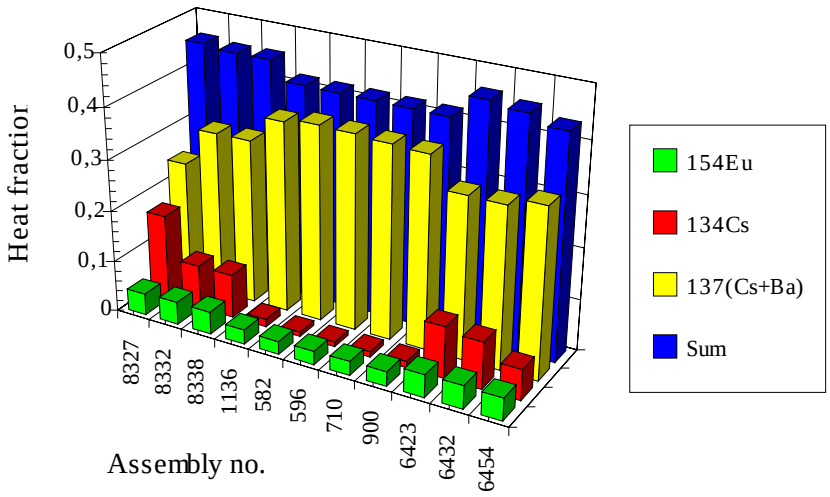

Figure 6. Fraction of the heat that arises from the gamma radiation from different isotopes and from the sum of the isotopes for the assemblies used here.

The diagrams of figure 7 show the gamma-fraction, f, as a function of CT for the isotopes ^{137}Cs, ^{134}Cs, ^{154}Eu and their sum. The value of f converges towards an almost constant value as the cooling time increases, as observed in reference [1]. figure 8 and figure 9 show the projected versions of figure 7 for ^{137}Cs and the sum. The curves of figure 8 are clearly separated into two groups, the upper one belonging to assemblies with low values of BU and ε and the lower one belonging to assemblies with high values of those parameters. The relative difference of these groups decreases from about 10 % at CT = 15 y to about 5 % at CT=50 y. The curves for the summed intensities, figure 9, show a smaller spread for CT:s in the 15 y range.

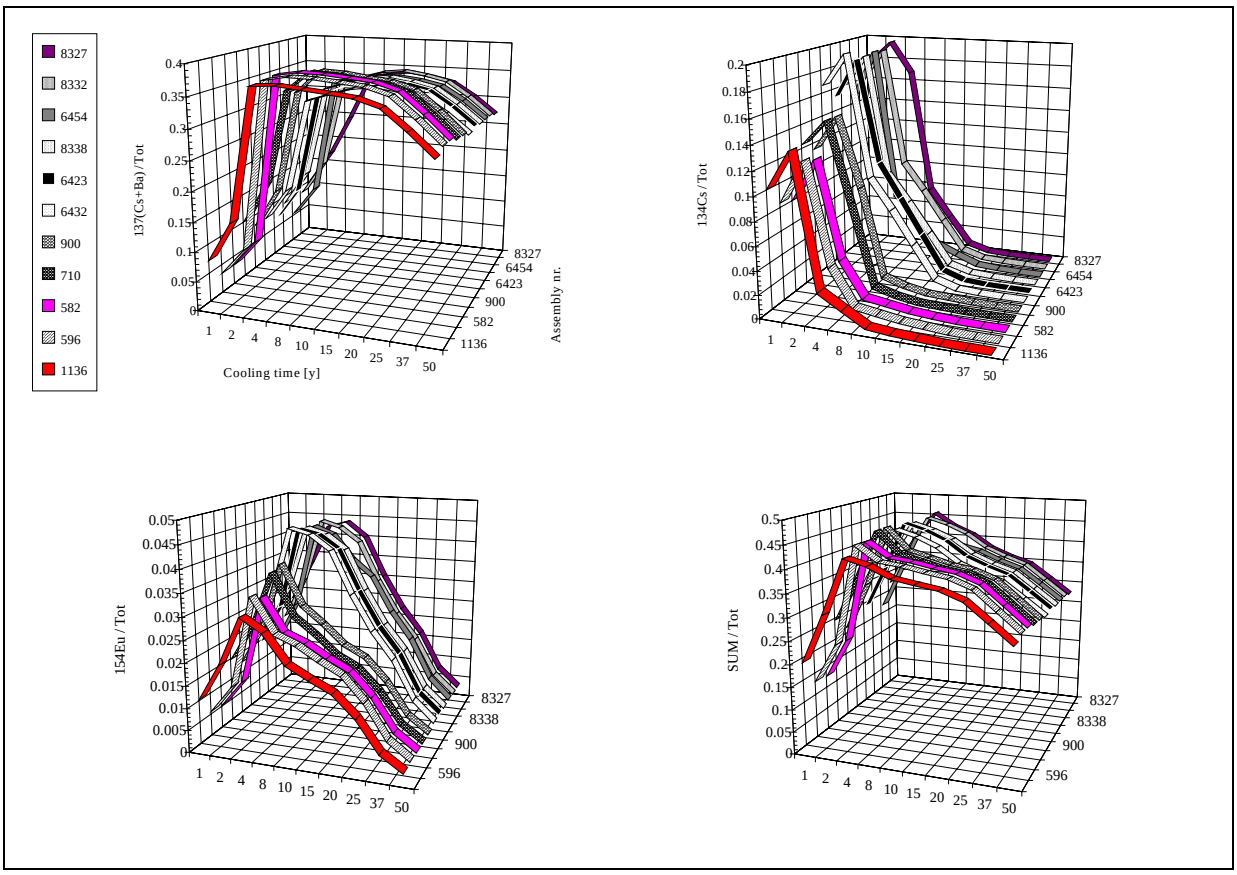

Figure 7. Time development of the heat fraction for the different isotopes and assemblies investigated.

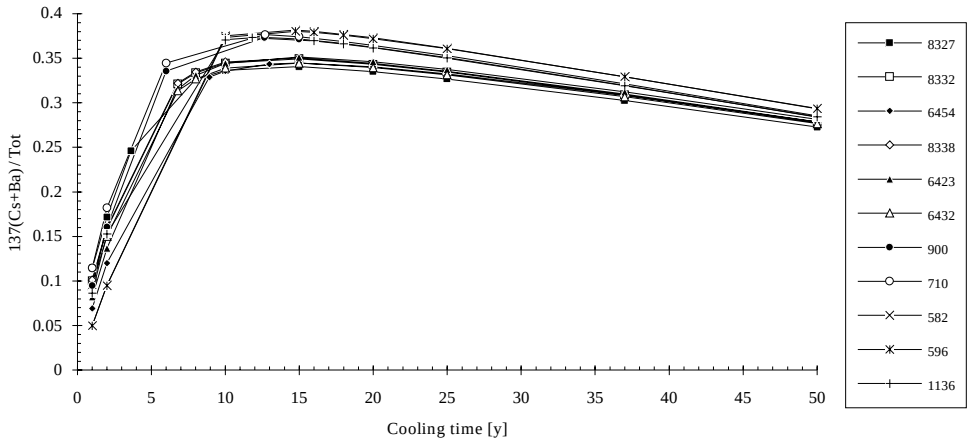

Figure 8. Time development of the heat fraction for ^{137}Cs.

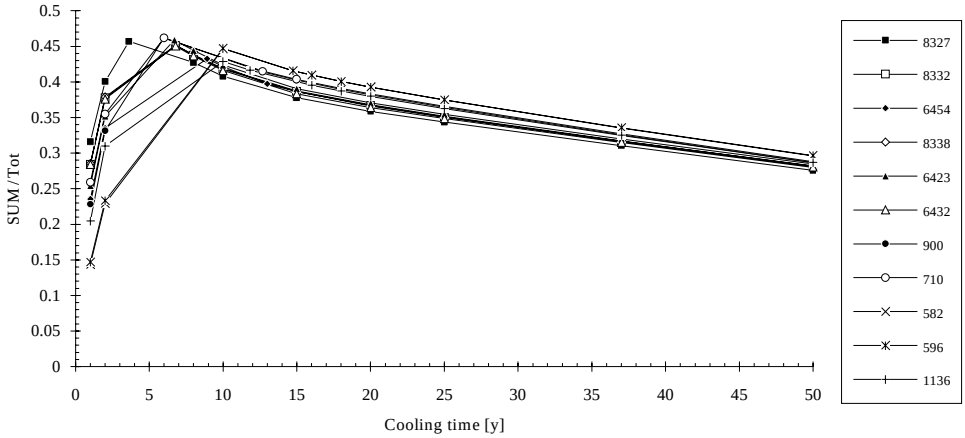

Figure 9. Time development of the heat fraction for the sum.

4 Gamma-Ray measurements

4.1 The Experimental Equipment

The equipment used in this work has been designed for determining the cooling time and burn-up of an assembly by means of gamma-ray spectroscopy. This equipment is installed at the storage facility CLAB at Oskarshamn, where the measurements in this work were performed. See e.g. references [2]-[3].

figure 10 shows a schematic picture of the installation of the gamma scanning equipment.

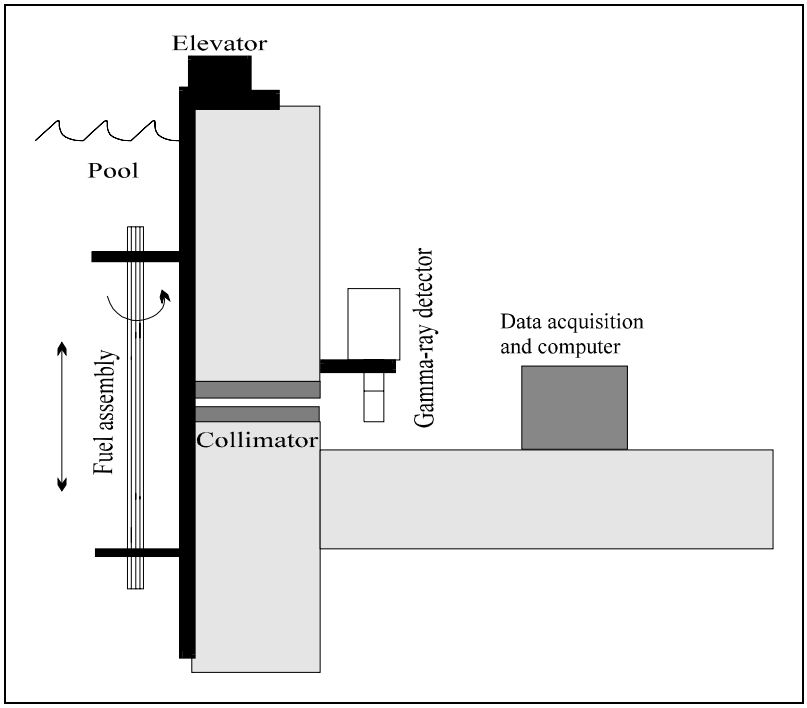

Figure 10. The experimental set-up.

Basically, the equipment consists of an elevator, a collimator and a high-resolution germanium detector. The fuel assembly to be investigated is placed in the elevator on the inside wall of a fuel handling pool and then moved up and down in front of the horizontal collimator in the pool wall. The assembly is fixed within ± 1 mm, (lateral directions), in the elevator and the fixture can be rotated 360° azimuthically with the aid of a stepping motor with a precision of about 0.2°.

The horizontal slit in the collimator allows the detector outside the wall to view a segment of the assembly with a height of a few cm and a width equal to the diagonal of the quadratic fuel assembly. When the assembly is mounted in the fixture, the distance between the detector and the centre of the fuel assembly is 246 cm. A distance of about 50 cm of water separates the fuel assembly and the pool wall. The transmission of gamma radiation in this region is about 1 % for 662 keV, (^{137}Cs).

Each corner of the assembly is scanned and a series of gamma-ray spectra is recorded using the data acquisition code SEDAS[‡]. The average of the gamma-ray intensities of all isotopes of interest over the whole fuel assembly is calculated and stored.

In figure 11 is a block diagram showing the electronic set-up and detector system used in this work.

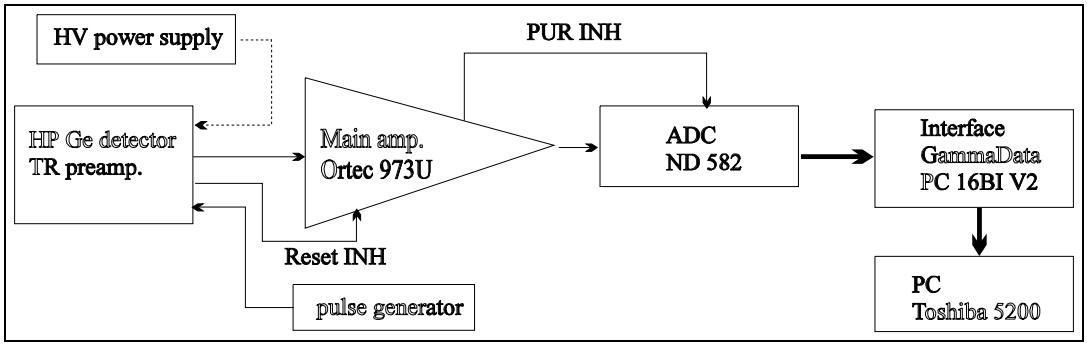

Figure 11. Schematic picture of the electronics.

After the pulses have been processed and digitised they are stored in a PC via a high-speed interface card.

The pre-amplifier is of the transistor reset type and the main amplifier is a gated integrator type Ortec 973U with 1.5 μs or 3.0 μs integration time. The ADC is of type ND 582 with a fixed nominal conversion time of 1.5 μs. (References [2] and [3] discusses the design and operation of this set-up in more detail.)

Before the experiment was carried out several performance parameters of the germanium detector was investigated. table 3 below shows the important parameters of the detector that was measured during this period. See appendix 6.1 for a fuller discussion and calculations of these parameters.

Performance parameter[§]	Value, (average of measured values).
FWHM	1.92 ± 0.02 keV
FWTM / FWHM	1.86 ± 0.02
FWFM / FWHM	2.45 ± 0.03
Peak-To-Compton ratio	60.2 ± 0.5
Relative efficiency	33.8 ± 0.9 %

Table 3. Summary of the performance parameters of the germanium detector.

[‡] Designed by 'Gammadata AB'.

[§] The parameters describe the peak of ^{60}Co at 1.33 MeV.

4.2 Experimental Results

figure 12 and figure 13 show the measured quantities that corresponds to the simulated values in chapter 3. These graphs are based on the tabulated values in appendix 6.5.

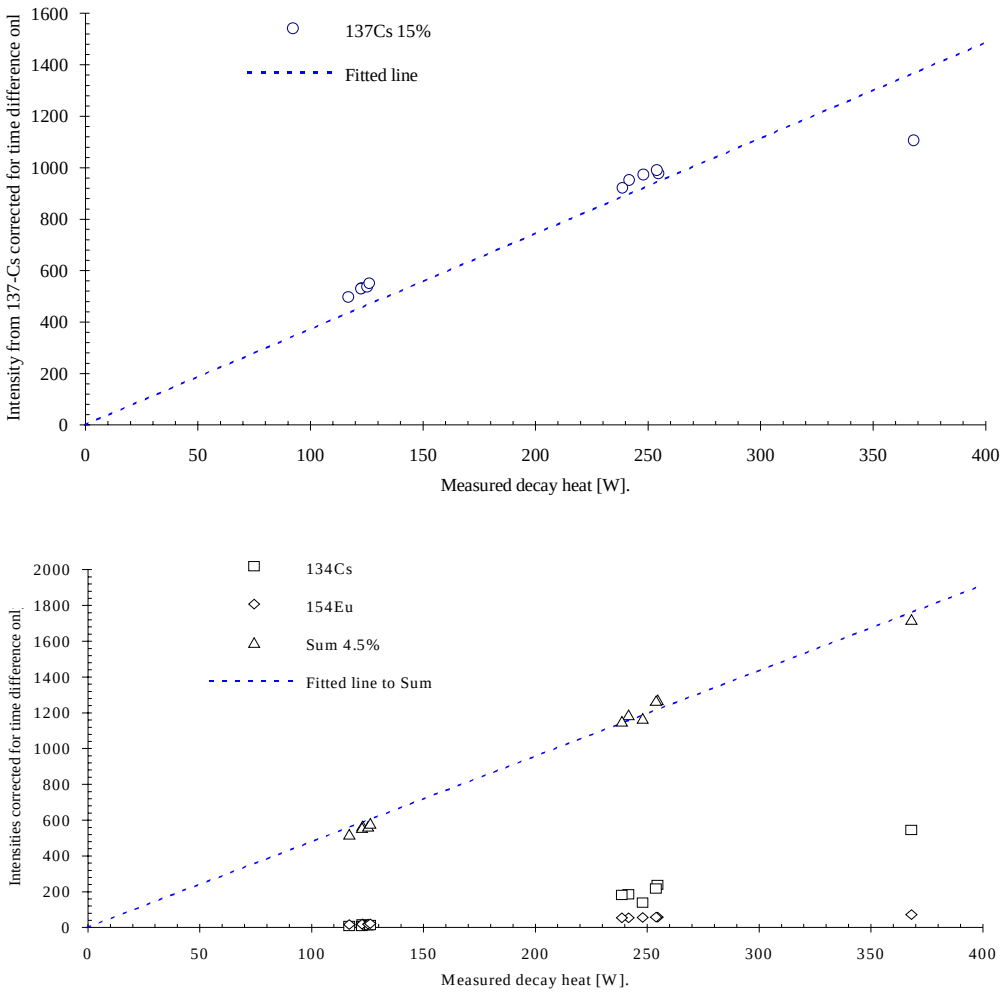

Figure 12. Measured intensities versus measured decay power. Here, no linearisation has been done.

figure 12 shows the measured intensities as a function of the calorimetrically measured decay heat. Here the intensities are only corrected for the difference in cooling time between the calorimetric measurements and the gamma scanning. The correlation between the intensity and decay heat is reasonably linear for ^{137}Cs, considering the different power histories, enrichments and the relatively short cooling times of the fuel assemblies.

If for some reason the cooling time should not be documented for an assembly and has to be determined experimentally the following treatment shows that the errors in the corrected intensities (using the standard value of the gamma-fraction *f*) will be reasonable small anyway.
The intensity of a decaying isotope as a function of time is written as

$$I=I_0 \cdot e^{-\lambda \cdot t} \qquad \textit{Eq 4}$$

Quadratic error summation results in the formula

$$\left(\frac{\Delta I}{I}\right)^2 = \left(\frac{\Delta I_0}{I_0}\right)^2 + (\lambda \cdot t)^2 \cdot \left[\left(\frac{\Delta \lambda}{\lambda}\right)^2 + \left(\frac{\Delta t}{t}\right)^2\right] \qquad \textit{Eq 5}$$

It is shown in reference [3] that it is possible to determine the cooling time of a fuel assembly with an error of 2 years when the cooling time of the assembly is lower than 50 years and 170 days when the cooling time is lower than 20 years, respectively. These figures refer to the case where nothing more but the type of fuel is known.
Assume a cooling time of ~40 years, i.e. t~40 years, and that Δt=2 years. Further, if $\Delta I_0 / I_0$ and $\Delta\lambda/\lambda$ is neglected in comparison with $\Delta t / t$, using ^{137}Cs gives an uncertainty in $\Delta I / I$ of about 4.6 %. This means that the errors in the corrected intensity from ^{137}Cs will be about 4.6 % in a worst case such as in this example.

figure 13 shows the intensities versus decay heat as in figure 12 but here the intensities are linearised by dividing with the fraction of the heat from the different isotopes, eq 2. This correction factor is calculated with the Origen2.1 code, as described in section 3.

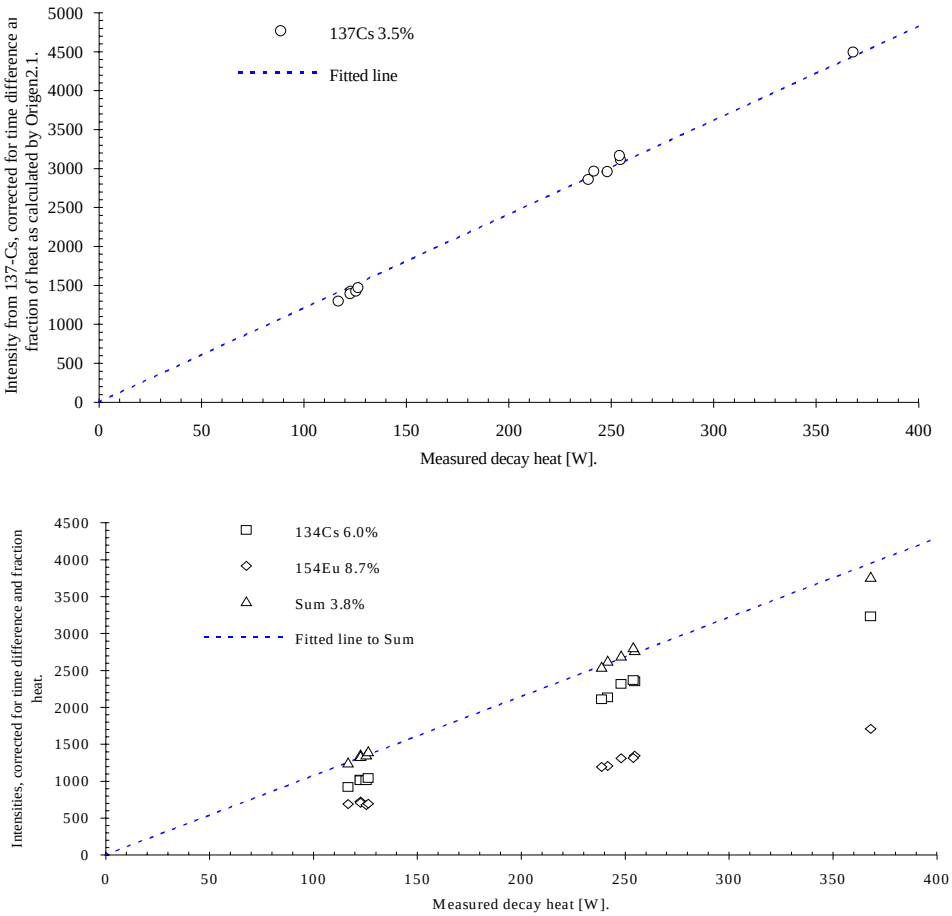

Figure 13. Linearised intensities versus decay power. Note the smaller deviation from straight lines as compared to the non-linearised case.

The linearity between intensities and decay heat in figure 13 is enhanced significantly and the deviations from straight lines are reduced correspondingly, i. e. 3.5 % for ^{137}Cs. The assemblies studied in this work have a comparatively short cooling time and the data points in the diagrams therefore scatter more than they are expected to do when the cooling times are about 40 years, see section 3. Even though the decay of ^{134}Cs and ^{154}Eu are supposed to be of limited use at the longer cooling times they are included here for completeness.

4.3 Conclusions of the Experimental Results

table 4 below shows a summary of the errors associated with the calibration of the gamma intensities from different isotopes versus decay heat.

Assumption	^{137}Cs	^{134}Cs	^{154}Eu	Sum
Only the cooling time is known.**	15 %	453 %	20 %	4.5 %
Power history and cooling time known, linerisation using Origen2.1 simulations.	3.5 %	6.0 %	8.7 %	3.8 %

Table 4. Comparison between the two cases considered in this thesis. The figures show the deviations from fitted straight lines.

To obtain an even smaller error in the calibration the decay heat has to be measured using a calorimeter that produces a more accurate value on this quantity since this is a major contribution to the errors here. The measured intensities are believed to be very accurate (standard deviation less than 1 %) compared to the measured decay heat. The linearisation factor used here has an estimated relative error of 3 %. This relatively small error will result in a small correction to the already relatively linear curve of intensity from ^{137}Cs vs. decay heat at cooling times of the order of 40 years.

** The cooling time can be determined (within two years) from gamma scanning according to ref. [3] under the assumption that no declared fuel parameters are available. (Here, no standard f-value is used.)

5 Calorimetric Measurement of the Decay Heat

As discussed above, the calorimetric measurements of the decay heat are essential for the calibration of the gamma-ray method. Such measurements have been performed by SKB at CLAB. In this report the heat loss due to escape of gamma radiation through the walls of the calorimeter is treated. An experimental measurement as well as a simple theoretical calculation of these losses have been made.

5.1 Calorimetric Measurement Procedure and Results

The calorimeter used at CLAB consists of a leak testing equipment[††] that is used to determine possible cracks in the spent nuclear fuel rods, see reference [5]. It essentially consists of a box of stainless steel that encloses the assembly that is to be investigated. In order to measure the decay heat from the fuel the following procedure is performed:

The fuel assembly is placed into the calorimeter and the temperature difference between the inside and outside water around the calorimeter is measured. This temperature difference is determined continuously over a period of time (of the order of twelve hours) until a stable difference is reached and the thermal flux through the calorimeter can be considered to be in steady state. The steady state temperature difference is then related to the heat produced by the spent nuclear fuel by using a calibration curve.

The calibration curve was accomplished by inserting a dummy assembly into the calorimeter. The fuel rods were heated electrically by an electrical wire with a well-known amount of power ranging from 0 to about 2 kW and the temperature difference was measured as described above. In this way a relation between the temperature difference and power produced is obtained.

The errors associated with the establishment of this calibration curve are not yet fully investigated /ref. [4]/ and significant deviations are noticeable at small heat powers.

So far fourteen assemblies have been measured in the calorimeter. The results are given in table 5.

[††] Called calorimeter throughout this work.

Assembly no.	Decay time [y]	Decay heat [W]. 1:st	2:nd	Relative difference [%]
8327	3.625	368.15		
8332	6.790	201.94	241.51	16.4
8338	6.790	240.08	238.7	0.6
1136	11.822	124.35	122.74	1.3
582	14.741	115.5	116.73	1.1
596	14.741	121.24	122.59	1.1
710	12.690	124.68	125.29	0.5
900	12.668	128.81	126.28	2.0
6423	6.691	254.56		
6432	6.784	257.77	253.87	1.5
6454	8.920	201.62	248.04	18.7

Table 5. Assemblies measured with the calorimetric method. Measured decay heat from reference [4]. Decay time means time from out of core to time of calorimetric measurement.

Most of the fuel assemblies were measured twice. With the exception of two assemblies the two data sets show good agreement, i. e. within 2%.

5.2 Missing Heat due to Gamma Radiation Leakage

The mechanical construction of the calorimeter allows some fraction of the gamma radiation from the fuel assemblies to escape the inner volume of the calorimeter. The energy that these quanta would have deposited inside the calorimeter is therefore lost and the measured temperature difference is lowered by the corresponding amount. In order to correct for this effect it is necessary to determine the amount of radiation that escapes the system.

This may be done either experimentally or by calculation. The experimental method applied here was a dose-rate measurement described in section 5.2.1. Since this experiment had some uncertainties its results were checked with an approximate calculation described in section 5.2.2.

5.2.1 Dosimetric Measurement of Gamma Radiation Leakage

The total thermal heat lost to the outside the calorimeter p_{esc} is obtained as an integral of the density of heat p(r) delivered by the gamma radiation over all space outside the calorimeter:

$$P_{esc.} = \iiint_{\text{Outside the assembly and box.}} p(\vec{r})dV \qquad \textit{Eq 6}$$

The power density can be written as the product $p=D\cdot\rho$, where D is the dose rate that a certain point outside the assembly is exposed to in water and ρ is the mass density of the water, 997 kg/m^3.

eq 6 can be rewritten as

$$P_{esc.} = \iiint_{\text{Outside}} D(\vec{r})\cdot\rho(\vec{r})dV = \rho \cdot \iiint_{\text{Outside}} D(\vec{r})dV \qquad \textit{Eq 7}$$

Here ρ is considered to be constant, (the temperature variations are considered to be small and their effect on ρ is therefore neglected).

The dose rate distribution D(r) was mapped with a dosimeter probe contained in a tube with dimensions shown in appendix 6.4. The probe was positioned as shown in figure 14. Several assemblies were measured axially and one assembly (6432) was measured also radially at a number of axial positions at two sides as indicated in figure 14. The results are tabulated in section 6.4.

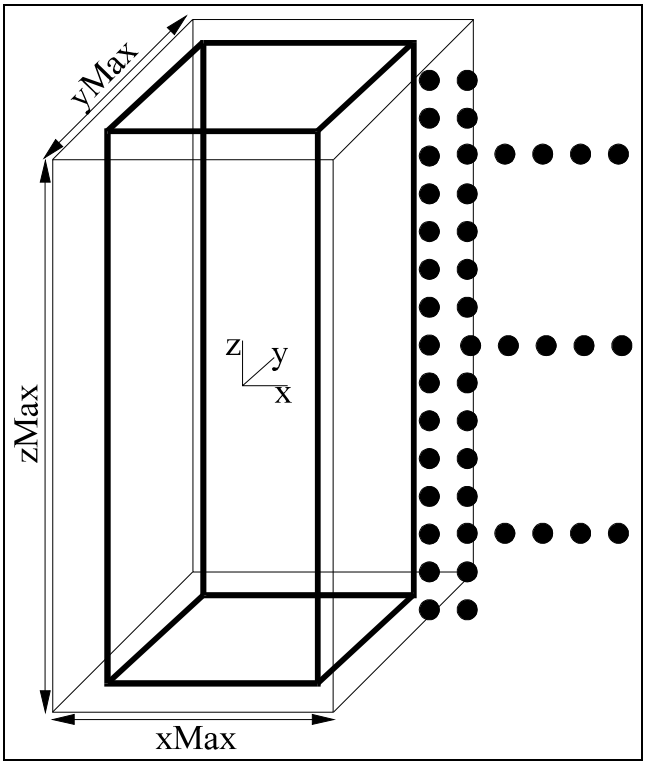

Figure 14. The dosimetric measurement performed on a fuel assembly inside the calorimeter. The black points represent the positions of the endcap of the container for the dosimetric probe.

The six complete radial distributions obtained are graphically represented in figure 15. The dose rate distribution is very similar for the two sides of the assembly but varies somewhat (15 %) in the axial direction. The radial distributions could all be fitted with simple exponentials with an attenuation constant close to 10 m^{-1} (this corresponds to the theoretical value for water for a radiation energy near 500 keV). The heavy line in figure 15 shows an average exponential distribution obtained from a fit to all six measured distributions.

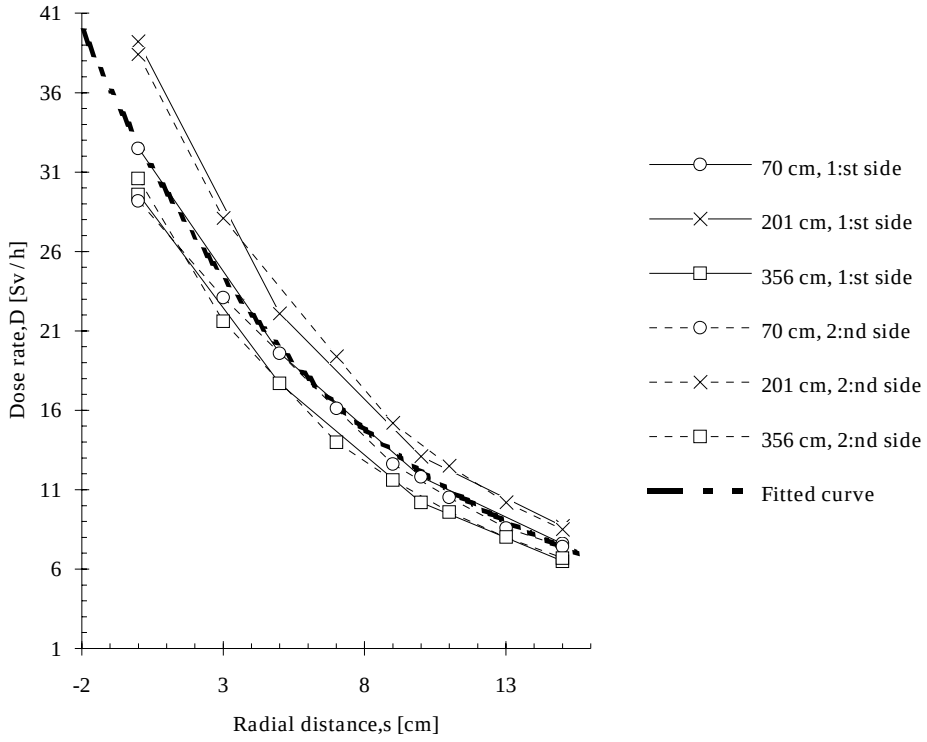

Figure 15. Resulting radial distributions of dose rates for assembly no 6432. The fitted curve was on the form $D \propto exp(-a \cdot s)$ where a is an average of the corresponding parameters in the individual cases.

The position of the dose-rate probe could only be varied axially and radially. Therefore, in order to evaluate eq 7, an assumption about the dose rate at various azimuthal angles had to be made. The dose rate was assumed to be constant as shown in figure 16, (only one of the lines of constant dose rate is drawn), to proceed with the calculations.

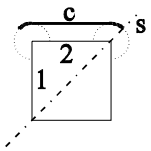

Figure 16. c is a line of constant dose rate and s is the diagonal line of symmetry in the fuel. 1 and 2 are sides of the assembly.

Furthermore, the burnup of the fuel was assumed to be symmetric in one of the diagonals. eq 7 then can be rewritten as

$$P_{esc.} = 2 \cdot \rho \cdot \iiint_{\substack{\text{Outside sides} \\ \text{1 and 2}}} D(\vec{r})dV \qquad \textit{Eq 8}$$

If the coordinate system of figure 29, (page 46), is introduced, eq 8 can be written with two terms, one for the sides and one for the corners:

$$P_{esc.} = 2\cdot\rho\cdot \iiint_{1+2} D(\vec{r})\,dV =$$

$$= \sum_{i=1}^{2} 2\cdot\rho\cdot\left(\int_{z=-zMax/2}^{zMax/2} \int_{y=-W/2}^{W/2} \int_{x=xMax/2}^{\infty} D_i \; dxdydz + \int_{z=-zMax/2}^{zMax/2} \int_{\varphi=0}^{\pi/2} \int_{r=d}^{\infty} D_i \; rdrd\varphi dz \right) \qquad \textit{Eq 9}$$

Here, D_i means the dose rate outside side i and φ is the angle at the corner of the calorimeter (not as in figure 29). It is also assumed that the dose rates are zero outside the top and bottom of the calorimeter, i.e. above $z = z_{max}/2$ and below $-z_{max}/2$. This assumption is reasonable when considering the large attenuation of the gamma radiation by the material in the top and bottom of the calorimeter. Due to the line of constant dose rate, the integral over y is calculated to be equal to W , which is the width of the assembly, 124.25 mm. d is the distance from the corner of the assembly to the corner of the calorimeter, 37.30 mm.

It was not possible to put the dosimetric probe directly onto the surface of the calorimeter due to its construction. The container for the relatively large probe was filled with air, see figure 36 on page 63, and an extrapolation of the radial measurement points had to be done towards the calorimeter. The form of the radial distribution of dose rates was written as

$$D_i(z)\cdot e^{-a\cdot(r-R)} \qquad \textit{Eq 10}$$

Here, R is, in a first approximation, the distance from the calorimeter to the center of the dosimeter probe, which was located about 11.3 cm from the end cap of the container of the probe, see figure 36 on page 63. However, the air-filled tube in front of the dosimeter probe will cause a higher reading of the dose rate than if water was present. Furthermore, the probe has a relatively large solid angle view of the calorimeter. This can be accounted for by introducing an effective value of R which is smaller than the geometric value. The size of this correction has here been very roughly estimated to about one cm and we therefore use $R = 10 \pm 0.5$ cm.

These assumptions implies that eq 9 can be written as

$$P_{esc.} = \sum_{i=1}^{2} 2\cdot\rho\cdot e^{aR}\cdot\left(W\cdot \int_{x=xMax/2}^{\infty} e^{-a(x-xMax/2)}\,dx + \frac{\pi}{2}\cdot\int_{r=d}^{\infty} e^{-ar}\,r\,dr\right)\cdot \int_{z=-zMax/2}^{zMax/2} D_i(z)\,dz = \qquad \textit{Eq 11}$$

$$= \sum_{i=1}^{2} 2\cdot\rho\cdot e^{aR}\cdot\left(W\cdot a^{-1} + \pi\cdot a^{-2}\cdot e^{-ad}\cdot(ad+1)/2\right)\cdot \int_{z=-zMax/2}^{zMax/2} D_i(z)\,dz$$

The integrals are calculated numerically from the axial distribution of the data. Since the measurements were carried out within a range less than z_{max}, an extrapolation was performed in order to extend the functions $D_i(z)$ to the integration limits of eq 11. Note that the integration in the z-direction was performed numerically with twelve points on each side and is therefore more accurate than the parameter a where only three different z-values were used on each side to calculate the average.

The resulting value of the escaping heat, $P_{esc.}$, from these calculations is 11 W (table 6), which means that about 9.5 % of the gamma radiation from assembly number 6432 escapes the calorimeter.

The errors in the measured dosimetric values are ± 10 % /ref. [7]/ and the calculated integrals are based on the measured distributions of dose rates including extrapolations of the obtained curves to zero dose rates, (in z-direction).

A rough estimate of the total error in the calculated thermal powers, $P_{esc.}$, is ± 15 %. This value is based somewhat on the scattering of the data points from the dosimetric measurement, but primarily on the uncertainty of the extrapolation procedures in the evaluation of eq 11.

5.2.2 Calculation of the Gamma Leakage with the Program TheFAT.

As is evident from the section above, the experimental determination of the gamma leakage suffers from some uncertainties. In principle it should be possible to accurately calculate the gamma leakage with a Monte Carlo calculation, but this would be complicated and time consuming. A rough calculation could be made in a simpler way as presented here.

The major contribution to the gamma-ray spectrum from the assemblies considered in this study arises from the decay of ^{137}Cs. Consider a ray of 662 keV gamma quanta travelling through the assembly as in figure 17.

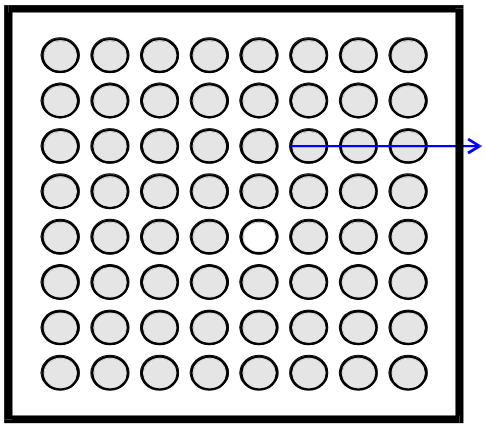

Figure 17. Sketch of an unboxed 8x8 BWR fuel assembly in the calorimeter.

Here the beam has to traverse three full lengths of uranium dioxide pellets surrounded by zircaloy tubes. The escaping fraction of this ray would, in the case it hits the walls perpendicularly, be approximately:

$$\exp\left[-6\cdot r_{UO_2}\cdot\mu_{UO_2}-5\cdot\left(r_{Zirc.}-r_{UO_2}\right)\cdot\mu_{Zirc.}-t_{H_2O}\cdot\mu_{H_2O}-t_{wall}\cdot\mu_{wall}\right]$$

Here r is the radius and t is the thickness of water and wall. Appendix 6.3 shows values of μ for the different materials and appendix 6.2.4 shows values of the radii and thickness of the fuel rods.

The result of this expression is that approximately 1 % of the primary gamma radiation escapes from this position in the direction perpendicular to the axis, (a numerical integration was performed here in the axial direction to account for the non-planar geometry of a real fuel assembly). An even larger fraction would escape if the gamma rays were radiating from a point closer to the surface of the calorimeter.

With this result at hand it is necessary to investigate the gamma radiation leakage further. For this purpose a computer simulation code was constructed.

The program TheFAT[#] was developed in order to simulate the leakage of gamma radiation from ordinary BWR fuel of the 8x8 type. These assemblies usually have one fuel rod in the centre removed.

The code essentially sets up a grid in a plane of the fuel assembly and sets attenuation coefficients at each grid point. The code also marks the grid points corresponding to radiating fuel rods. A simple ray-trace algorithm is then executed where the program sends out rays at every radiating grid point in several different directions in the plane. Each ray corresponds to a collimated beam of gamma rays.

To account for the non-planar geometry in this program a continous distribution of gamma rays was used in the axial direction of the fuel. This correspond to performing a numerical integration and taking care of the angular dependence of the attenuation of the gamma rays.

The algorithm calculates the leakage fraction for each ray, using the formula for attenuation of primary gamma rays, $I=I_0\cdot\exp\{-\mu\cdot x\}$. Finally, an average is calculated of all leakage fractions from every ray. This

[#] TheFAT=theoretical correction factor for self attenuation, written in the programming language Fortran90.

average is defined as the leakage fraction of the whole assembly. This procedure is performed for the gamma ray energies of interest.

Appendix 7.2 discusses in greater detail the simulations and assumptions made to generate an executable code.

Results and error estimates from the simulations of escaping gamma rays

The program was executed for 20 gamma-ray energies using different grids and various divisions of emission angles at every grid point to investigate the stability of the algorithm. The results from these simulations are shown in figure 18, which are drawn on the basis of the tabulated values in appendix 5.2.3.

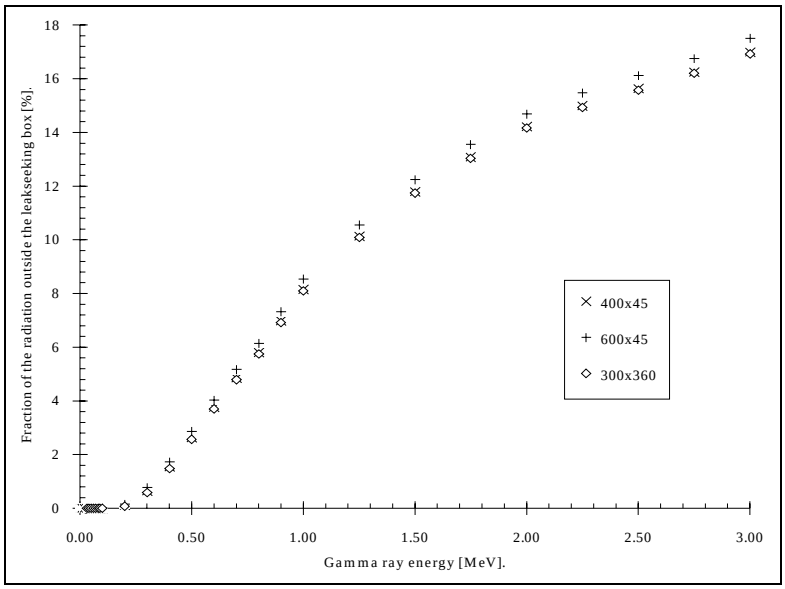

Figure 18. Results from the simulation of gamma escape fraction. The legend corresponds to the number of gridpoints versus the number of angles used in the simulation.

Using these results it is possible to obtain a weighted average of the escape fraction for individual fuel assemblies, using the energy spectra from the gamma scanning experiment. Below, in figure 19, is a graph based on the values in appendix 6.2.5, of these fractions for the assemblies that was examined in this thesis.

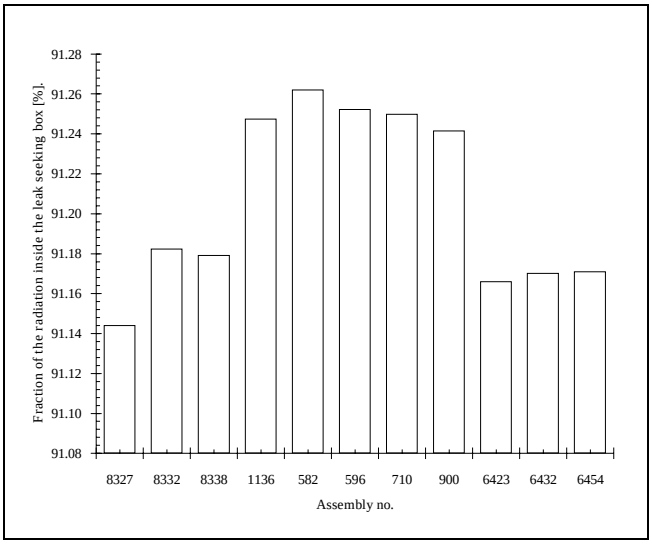

Figure 19. Fraction of gamma radiation that remains inside the calorimeter. The numbers on the abscissa are the identities of the assemblies studied in this work.

The program TheFAT calculates the escape fraction of the primary gamma radiation, ignoring scattering of the photons. This might seem like a crude approximation but, as will be shown below, the correction factors[§§] for these effects are close to unity and the approximation can therefore be justified. Reference [8] discusses the use of primary gamma's in some detail.

Since the major contribution to the gamma-ray spectra comes from ^{137}Cs, this is the energy that will be treated below. Thus the energy of the gamma radiation is 661.65 keV.

Reference [9] gives the exposure dose build-up factor in lead for a point isotropic source. Lead is used as a fair approximation of UO_2 in this context. Assuming a relaxation length of $\mu_{Pb} \cdot R \approx 121 \cdot 1.0 \cdot 10^{-2} \approx 1.2$ a build-up factor of about 1.3 is obtained from ref. [9]. Here R is the distance the gamma ray travels through the lead and μ_{Pb} is the linear attenuation coefficient of lead, /ref. [10]/. R is assumed to be 1 cm but in reality it is smaller and the build-up factor will be closer to unity.

This treatment shows that it is possible to ignore the secondary effects on the gamma radiation in a first approximation. Still the simulation will show an approximation of the total leakage fraction that is fairly close to the correct value. Using build-up factors in the simulation code will probably give a more precise value. However, in this work there was no reason to go further in accuracy.

The major contributor to the total error comes from the uncertainty of the build-up factors. The relative errors of the results from the simulation code is estimated to be less than 15 %. Furthermore, the build-up factor that should be used to correct the simulated values is assumed to be in the order of 1.15. The computational errors, from floating point manipulations, truncation and the finite sized grid are the main contributions to the errors of the primary radiation escape fractions. These effects are small in comparison with the errors associated with the build-up factors.

[§§] Called the 'Build Up' factors.

5.2.3 Comparison Between Simulations and Measurements

The gamma radiation contributes with a fraction f to the total thermal power in the spent fuel. Therefore, to be able to compare the simulated values with the measured values it was decided to use the escaping fraction as a way of comparison, since this was calculated directly in the simulations and it was preferred not to manipulate these values even more with calculated values.

table 6 below summarises the results of the dosimetric measurements and the simulations for assembly 6432. Here column 4 and 5 show the results of the dosimetric measurements (See section 6.4.). Column 5 shows the escaping fraction of the heat from the gamma radiation and is calculated from

$$P_{total} = P_{esc.} + P_{calorimetric} \qquad \textit{Eq 12}$$

$$P_{\gamma} = f \cdot P_{total} \qquad \textit{Eq 13}$$

Here, f is the fraction of the heat that arises from the gamma radiation. (This fraction is simulated using the Origen2.1 code. Note that f here is the fraction from the total gamma radiation.)

$$\Rightarrow \quad \frac{P_{esc.}}{P_{\gamma}} = \frac{P_{esc.}}{f \cdot P_{total}} = \frac{P_{esc.}}{f \cdot \left(P_{esc.} + P_{calorimetric}\right)} = \frac{1}{f \cdot \left(1 + P_{calorimetric} / P_{esc.}\right)} \qquad \textit{Eq 14}$$

The last column gives the result of the simulated calculation described in section 6.2.2. Considering the relatively large uncertainties involved in both methods the two methods agree very well, indicating a ”true” value of the gamma-ray escape fraction of about 9.6 %. This corresponds to 4 % of the total decay heat. Furthermore, the value of f is approximated by the fraction of the heat that arises from the sum of the intensities from ^{137}Cs, ^{134}Cs and ^{154}Eu.

Ass. no.	Decay heat [W] *	f	$P_{esc.}$ [W]	$\Rightarrow P_{esc.} / P_{\gamma}$ [%]	Sim. frac. [%] **
6432	253.87	0.45	11.1 ± 1.7	9.3 ± 1.3	10.1 ± 1.5

*Table 6. Results from the dosimetric measurements and comparison with the simulated escape fractions**, of the heat from the gamma radiation. * Calorimetric measured heat. The simulated fraction is based on the simulated value 8.8 % and corrected for the build-up by 15 %.*

5.2.4 Possible Improvements

One improvement of the calorimeter would be to increase the gamma attenuation of the calorimeter. The measurements show that as much as about 9 % of the heat from gamma radiation leaks out from the calorimeter. To improve the absolute determination of decay heat, this gamma radiation should be confined inside the calorimeter.

6 Appendices

6.1 The Germanium Detector and it's Performance

figure 20 shows a typical spectrum produced by the germanium detector used in this work.

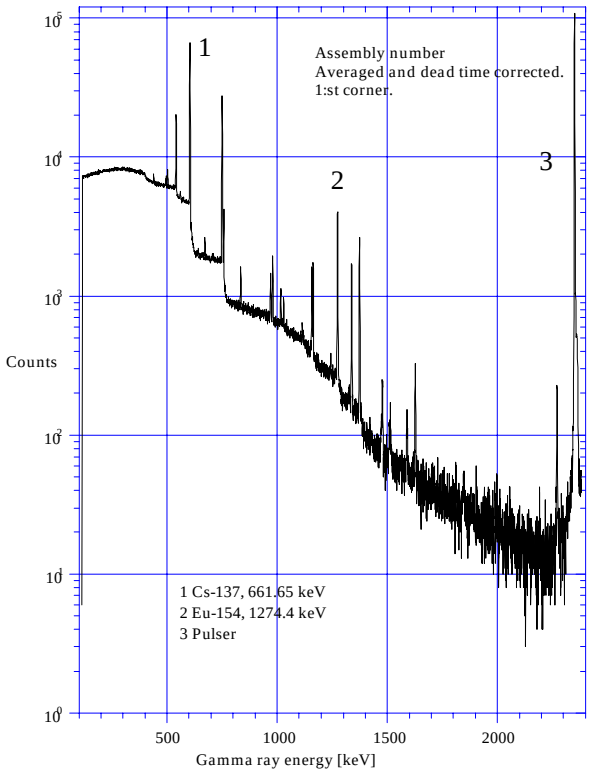

Figure 20. Typical spectrum from the germanium detector.

figure 20 illustrates the importance of high energy resolution. The detector used has a resolution of better than 2 keV at 1.33 MeV.

As described in reference [2], a high throughput of the detector system is important in order to register weak activities in the presence of strong ones. This is especially important if the measuring system is used for determining cooling time and burn-up.

This is accomplished by using a transistor reset preamplifier, a gated integrator main amplifier and a specially designed interface card between the ADC and the computer, reference [2].

Preliminary tests of the germanium detector were performed before the experiment with focus on the resolution and throughput of the experimental set-up. The following four subchapters account for these tests.

6.1.1 Resolution

The resolution of individual peaks is critical in the performance of the gamma scanning method. In figure 21 is some definitions used in the calculations of different resolution parameters.

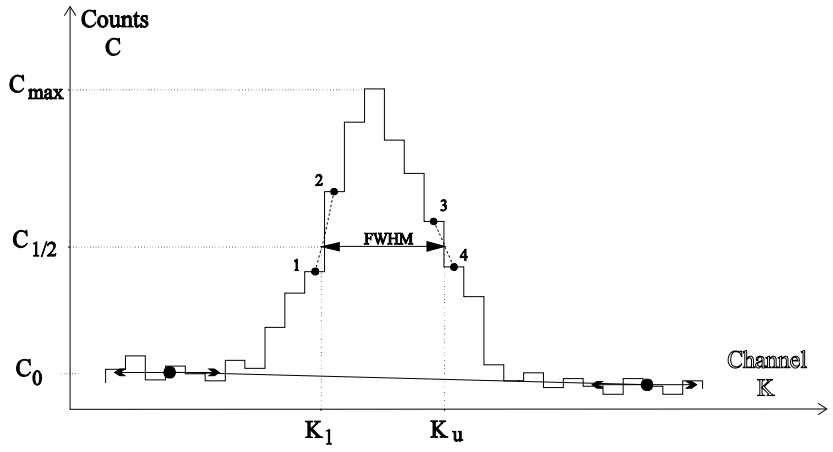

Figure 21. Definitions used to calculate FWHM. C_0 represent the zero level of counts to define C_{max} , when the background around the peak is defined as the line between the averages of counts between the four arrowheads.

To calculate FWHM[***] for a peak in the gamma ray spectrum the following procedure was carried out:

1) Fit the background line to the defined regions below and above the peak, (figure 21).
2) Subtract the background from the collected spectrum.
3) Calibrate the spectrum and save the calibration parameters.
4) Save the value of C_{max} and calculate $C_{1/2}=C_{max}/2$
5) Calculate the equations for the straight lines between the points 1,2 and 3,4 respectively. Line 1: $C(K)=\left(\frac{C_1-C_2}{K_1-K_2}\right)\cdot(K-K_1)+C_1$, line 2: $C(K)=\left(\frac{C_3-C_4}{K_3-K_4}\right)\cdot(K-K_3)+C_3$.
6) Calculate FWHM as the distance between the lines, see figure 21. $FWHM=K_u-K_l = =\left[\left(\frac{C_{1/2}-C_3}{C_3-C_4}\right)\cdot(K_3-K_4)+K_3\right]-\left[\left(\frac{C_{1/2}-C_1}{C_1-C_2}\right)\cdot(K_1-K_2)+K_1\right]$
7) Calculate FWHM in energy scale using the calibration.

Some standard values are often calculated to be able to manifest the quality of the detector and to be able to compare different detectors to each other. These are the ratios $\frac{FWTM}{FWHM}$, $\frac{FWFM}{FWHM}$ and the peak-to-compton

[***] FWHM=full width at half maximum, To calculate full width at tenth maximum (FWTM) and full width at fiftieth maximum (FWFM) an analog procedure is performed where, for instance, $C_{1/2}$ is replaced $C_{1/10}$ or $C_{1/50}$ etc.

ratio. The peak-to-Compton ratio is defined as the ratio between the peak value in the full energy peak and the average number of counts in the Compton plateau, i.e. the part of the spectrum that contains events from Compton scattered photons.

The ratios involving FWHM describe how well the peak corresponds to a pure Gaussian shape. For a Gaussian the following values apply:

$$\frac{\mathrm{FWTM}}{\mathrm{FWHM}} = \sqrt{\frac{\ln(10)}{\ln(2)}} \approx 1.823 \quad \text{and} \quad \frac{\mathrm{FWFM}}{\mathrm{FWHM}} = \sqrt{\frac{\ln(50)}{\ln(2)}} \approx 2.376 .$$

The detector parameters above were measured using the peak at 1.33 MeV from a ^{60}Co source. The Compton plateau was defined between 1040 and 1096 keV. The experimentally obtained values were compared with the values stated by the manufacturer, see table 8.

figure 22 below shows two plots of the measured quantities

.

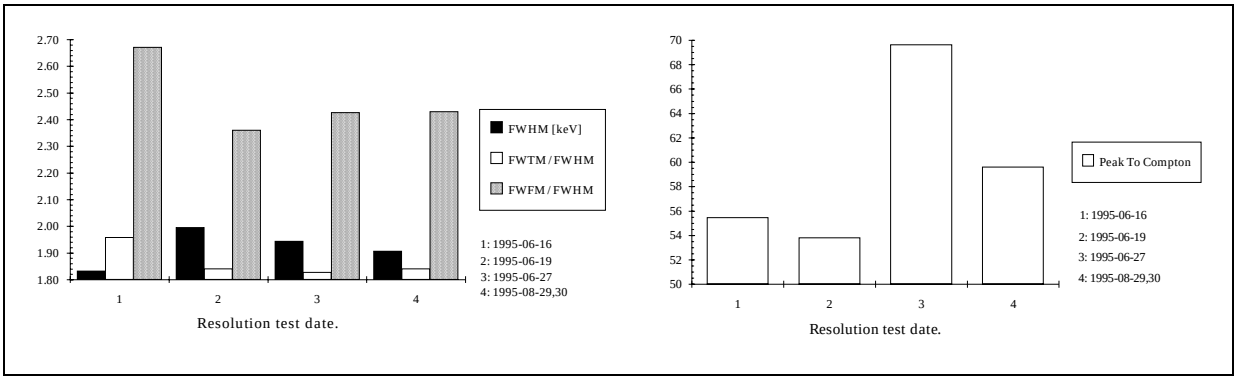

Figure 22. Results from the performance measurements.

The graphs in figure 22 were generated using the measured information that is supplied in appendix 6.1.2. The warranted values from the manufacturer can also be found in appendix 6.1.2. The parameters of the detector is seen to scatter around a mean value. However, the test that was performed on 1995-06-27 shows a large peak-to-Compton ratio as compared to the other dates. This is explained by the fact the background subtraction was different in this case. Here, a spectrum was collected without any source of radioactivity besides the normal background. This spectrum was then subtracted from the spectrum with a source before the procedure explained above was carried out. This influences the Compton plateau and, in turn, influences the peak-to-Compton ratio. It should be noted that this latter method usually should be performed if the background rate is high compared to the rate from the source to get a spectrum that is easier to work with in the procedure above.

An unexpected circumstance influencing the behaviour of the performance parameters was the humidity of the air around the detector. A large humidity had a negative effect on all parameters above but the detector always had performance parameters that were better than the warranted values.

6.1.2 Resolution Test Data and Warranted Values

table 7 below shows the measured values obtained in the resolution tests of the germanium detector, using a spectroscopy amplifier (model 673 from ORTEC), and the resulting values of the performance parameters of the detector. The amplifier has two modes of operation, gaussian and gated integrator. Here the amplifier was used in the gaussian mode. table 8 shows the warranted and measured values of the detector parameters, (as specified by the manufacturer of the detector).

Date		1995-06-16	1995-06-19	1995-06-27	1995-08-29,30
Calibration parameters (E=k·CH+m) CH1(cen)		3299.788	3299.863	3301.564	4005.119
E1=1332.5 keV,E2=1173.2 keV	CH2(cen)	2907.213	2907.23	2908.897	3528.112
Background around 1332 keV	below	3	6	7	27
	above	3	3	3	6
C_{max} (At 1332 keV.)		945	2036	4387	14072
FWHM	K1	3297	3297	3299	4002
	C1	330	766	1941	6034
	K2	3298	3298	3300	4003
	C2	600	1360	3346	9426
	K3	3302	3302	3303	4008
	C3	485	1234	3621	7072
	K4	3303	3303	3304	4009
	C4	265	617	2162	3882
FWTM	K1	3295	3295	3297	3999
	C1	76	141	344	630
	K2	3296	3296	3298	4000
	C2	151	339	948	1538
	K3	3304	3304	3305	4010
	C3	107	292	968	1863
	K4	3305	3305	3306	4011
	C4	32	76	399	730
FWFM	K1	3293	3293	3295	3998
	C1	7.1	20	33	270
	K2	3294	3294	3296	3999
	C2	24	44	115	630
	K3	3306	3305	3307	4011
	C3	21	76	129	730
	K4	3307	3306	3308	4012
	C4	7.1	29	27	276
Average between 1040 & 1096 keV - bgr		17	37	63	236
1332 peak - bgr		943	1991	4387	14066
Resulting calculated parameters follow:					
FWHM [keV]		1.83±0.04	2.00±0.04	1.94±0.04	1.91±0.03
FWTM/FWHM		1.96±0.05	1.84±0.04	1.83±0.04	1.84±0.04
FWFM/FWHM		2.67±0.06	2.36±0.05	2.43±0.05	2.43±0.05
Peak To Compton ratio		55.5±3.7	53.8±1.9	69.6±1.5	59.6±0.6
ε_r [%]		33.8±0.9			

Table 7. Measured and calculated parameters regarding the performance of the germanium detector.

Parameter	Warranted value	Measured value[†††]	Our measurements
FHWM at 1.33 MeV, ^{60}Co	2.31 keV	1.75 keV	1.92±0.02 keV
Peak-to-Compton Ratio, ^{60}Co	48.7	60.1	60.3±0.5
ε_r at 1.33 MeV, ^{60}Co	32.4 %	35.3 %	33.8±0.9
FWTM / FWHM, ^{60}Co	2.00	1.88	1.86±0.02
FWFM / FWHM, ^{60}Co	3.00	2.49	2.45±0.03

Table 8. Warranted and measured performance parameters from the manufacturer of the detector. Also shown is the average values of our mesurements.

To calculate the errors in table 7 above it was assumed that the errors in the determination of channel number is in the order of 1/10 of a channel. For example,

$\Delta(\mathrm{FWXM}) = \Delta E$, where $\Delta E = \mathrm{abs}(\partial E/\partial K)\cdot(\Delta K)$ and $\Delta K \approx 1/10$ channels. Here, FWXM means FWHM, FWTM or FWFM. This results in the following error formula for FWXM:

$$\left(\Delta\left(\frac{\mathrm{FWXM}}{\mathrm{FWHM}}\right)\right)^2 = \left(\partial\left(\frac{\mathrm{FWXM}}{\mathrm{FWHM}}\right)\Big/\partial\mathrm{FWXM}\right)^2\cdot(\Delta\mathrm{FWXM})^2 + \left(\partial\left(\frac{\mathrm{FWXM}}{\mathrm{FWHM}}\right)\Big/\partial\mathrm{FWHM}\right)^2\cdot(\Delta\mathrm{FWHM})^2$$

$$\Rightarrow \quad \left(\Delta\left(\frac{\mathrm{FWXM}}{\mathrm{FWHM}}\right)\right)^2 \Big/ \left(\frac{\mathrm{FWXM}}{\mathrm{FWHM}}\right)^2 = (\Delta\mathrm{FWXM})^2/(\mathrm{FWXM})^2 + (\Delta\mathrm{FWHM})^2/(\mathrm{FWHM})^2$$

6.1.3 Efficiency

One important aspect of the detector is it's gamma detection efficiency. Two types of efficiencies can be defined, absolute or total efficiency and intrinsic efficiency. The definition of these efficiencies (ε_{abs} and ε_{int}) follows:

$$\begin{cases} \varepsilon_{abs} = \dfrac{\text{Number of pulses recorded}}{\text{Number of quanta emitted by the source}} \\ \varepsilon_{int} = \dfrac{\text{Number of pulses recorded}}{\text{Number of quanta incident on detector}} \end{cases} \qquad \text{(isotropic source)}$$

Note that that ε_{int} does not contain the solid angle as seen by the radiating source towards the detector. For a large distance between source and detector, ε_{abs} and ε_{int} are related by the expression

$$\varepsilon_{abs} = \varepsilon_{int}\cdot\frac{\Omega}{4\pi} \qquad \textit{Eq 15}$$

Here Ω, the solid angle, is defined (see page 117 of reference [11]) as

$$\Omega = \iint_A \frac{\cos(\alpha)}{r^2}\,dA\,, \qquad \textit{Eq 16}$$

where α and r are the quantities shown in figure 23 below.

[†††] Measured by the manufacturer 1995-05-05.

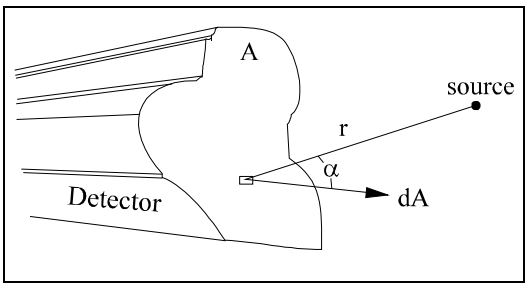

Figure 23. General detector geometry.

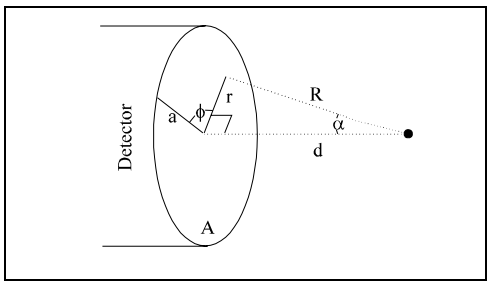

Figure 24. Cylindrical detector geometry.

The efficiency of the detector is given as a relative efficiency (ε_r), that is, the ratio between the absolute efficiency of the detector and a standard absolute efficiency. The standard that is used is a measured efficiency of a cylindrical 3"×3" NaI detector for 1.33 MeV radiation from a calibrated source of ^{60}Co placed on the line of symmetry of the detector at a distance of 25 cm from the end cap of the detector, see figure 24 above. This absolute efficiency is $1.2 \cdot 10^{-3}$.

With a cylindrical detector and the source on the line of symmetry, where a is the radius of the detector and d is the distance to the end cap of the detector, as in figure 24, Ω is calculated as

$$\Omega = \iint_A \frac{\cos(\alpha)}{r^2}\,dA = \int_0^a \int_0^{2\pi} \frac{1}{R^2} \cdot \frac{d}{R}\,r\,dr\,d\varphi = \int_0^a \int_0^{2\pi} \frac{1}{r^2+d^2} \cdot \frac{d}{\sqrt{r^2+d^2}}\,r\,dr\,d\varphi = 2\pi d \cdot \int_0^a \frac{r\,dr}{\left(r^2+d^2\right)^{3/2}} = 2\pi \cdot \left(1 - \frac{d}{\sqrt{d^2+a^2}}\right)$$

When d >> a, this formula can be approximated as

$$\Omega = 2\pi \cdot \left(\frac{\sqrt{d^2+a^2}-d}{\sqrt{d^2+a^2}}\right) = \frac{2\pi a^2}{d^2} \cdot \left(\frac{d^2}{a^2} \cdot \frac{\sqrt{d^2+a^2}-d}{\sqrt{d^2+a^2}}\right) = \frac{2\pi a^2}{d^2} \cdot \left(\frac{d^2}{a^2} \cdot \frac{d \cdot \left(\sqrt{1+a^2d^{-2}}-1\right)}{d\sqrt{1+a^2d^{-2}}}\right) \approx \frac{2\pi a^2}{d^2} \cdot \left(\frac{d^2}{a^2} \cdot \frac{1+a^2d^{-2}/2-1}{1}\right) = \frac{A}{d^2}$$

Since the geometrical errors are small and centred around zero, the quadratic error summation can be used.

$$(\Delta\Omega(a,d))^2 = \left(\frac{\partial\Omega}{\partial a}\right)^2 \cdot (\Delta a)^2 + \left(\frac{\partial\Omega}{\partial d}\right)^2 \cdot (\Delta d)^2 = \left(2\pi a d^{-2} \cdot \left(1+a^2d^{-2}\right)^{-3/2}\right)^2 \cdot (\Delta a)^2 + \left(-2\pi a^2 d^{-3} \cdot \left(1+a^2d^{-2}\right)^{-3/2}\right)^2 \cdot (\Delta d)^2 =$$

$$= 4\pi^2 \cdot \left(1+a^2d^{-2}\right)^{-3} \cdot \left(a^2d^{-4} \cdot (\Delta a)^2 + a^4d^{-6} \cdot (\Delta d)^2\right)$$

$$\begin{cases} d = 25\text{cm} \pm 0.1\text{cm} \\ a = 28.05\text{mm} \pm 0.1\text{mm} \end{cases}$$

$\Rightarrow \quad \Omega \approx 0.0392 \pm 0.0004$ sr. $\approx 4\pi \cdot (\, 3.12 \pm 0.04\,) \cdot 10^{-3}$ sr.

The relative efficiency is calculated according to the measurement made 1995-06-16 as

$$\varepsilon_r = \frac{\varepsilon_{abs}(\mathrm{Ge})}{\varepsilon_{abs}(\mathrm{NaI})} = \frac{(\text{peak area}) \,/\, (\text{activity} \cdot \text{live time})}{1.2 \cdot 10^{-3}}$$

where the activity is a calibrated ^{60}Co source and the peak area means the area of the 1332 keV peak.

Calibration parameters: $\begin{cases} \text{Activity, } A(1988\text{-}12\text{-}01,\ 12{:}00\ \mathrm{GMT}) = 396\ \mathrm{kBq} \\ T_{1/2}\left(^{60}\mathrm{Co}\right) = 5.27\ \mathrm{y} \\ \Delta A(1988\text{-}12\text{-}01) \approx 1.9\ \% \end{cases}$

$$\Rightarrow \quad A(1995\text{-}06\text{-}16) = A(1988\text{-}12\text{-}01) \cdot \exp\left(\frac{-t \cdot \ln 2}{T_{1/2}} \right)\Bigg|_{\substack{t=\text{time diff. between} \\ \text{the two dates} \approx 6.54\mathrm{y}}} \approx 167.5\ \mathrm{kBq}\ \ (\pm 3.18\ \mathrm{kBq})$$

Here, the errors in the time parameters are ignored.

Measured quantities: $\begin{cases} \text{peak area} = 33547\ \text{counts} \\ \text{rate}_{\text{pulser peak}} \approx 943.59\ \text{cps} \\ \text{dead time correction factor} = \text{rate}_{\text{pulser}} \,/\, \text{rate}_{\text{pulser peak}} = 1000 \,/\, 943.59 \approx 1.05978 \end{cases}$

$$\Rightarrow \quad \varepsilon_r \approx \frac{33547 \cdot 1.05978}{1.2 \cdot 10^{-3} \cdot \left(167.5 \cdot 10^3\, \mathrm{s}^{-1} \cdot 524\mathrm{s}\right)} \approx 33.75\ \%$$

$$\begin{cases} \varepsilon_{absolute} \equiv \varepsilon_a = \varepsilon_{int\,rinsic} \cdot \dfrac{\Omega}{4\pi} \equiv \varepsilon_i \cdot \dfrac{\Omega}{4\pi} \quad \Rightarrow \quad (\Delta\varepsilon_a)^2 = (\Delta\varepsilon_i)^2 \cdot \left(\dfrac{\partial \varepsilon_a}{\partial \varepsilon_i} \right)^2 + (\Delta\Omega)^2 \cdot \left(\dfrac{\partial \varepsilon_a}{\partial \Omega} \right)^2 \\ \text{But, } \varepsilon_a = \dfrac{\text{Rate}_{\text{peak}}}{\text{Activity}} \equiv \dfrac{R}{A} = \varepsilon_i \cdot \dfrac{\Omega}{4\pi} \quad \Rightarrow \quad \varepsilon_i = \dfrac{R \cdot 4\pi}{A \cdot \Omega} \end{cases}$$

$$\Rightarrow \quad (\Delta\varepsilon_a)^2 = (\Delta\varepsilon_i)^2 \cdot \left(\frac{\Omega}{4\pi} \right)^2 + (\Delta\Omega)^2 \cdot \left(\frac{\varepsilon_i}{4\pi} \right)^2 = \varepsilon_a^2 \cdot \left[\left(\frac{\Delta R}{R} \right)^2 + \left(\frac{\Delta A}{A} \right)^2 + 2 \cdot \left(\frac{\Delta\Omega}{\Omega} \right)^2 \right]$$

$$\begin{cases} \dfrac{\Delta A}{A} = 1.9\ \% \\ \dfrac{\Delta R}{R} = \dfrac{\sqrt{33547}}{33547} \\ \dfrac{\Delta\Omega}{\Omega} \approx \dfrac{0.0004}{0.0392} \end{cases} \qquad \Rightarrow \qquad \Delta\varepsilon_r = \frac{\Delta\varepsilon_a}{\varepsilon_a(\mathrm{NaI})} \approx 8.38 \cdot 10^{-3}$$

$\therefore \quad \varepsilon_r \approx 33.8 \pm 0.9\ \%$

This is better than the warranted value, (appendix 6.1.1).

6.1.4 Throughput

Throughput is most often accounted for as a graph over the output rate as a function of the input rate. To measure the different rates the set-up shown in figure 25 was used. The pulser was included as tool to perform a dead-time measurement of this system. The dead ”time” of the system here is defined as the ratio between the number of pulses recorded in the pulser peak in the spectrum and the known number of pulses put in the detector (the frequency of the pulser and the collection time was known). The dead time study was not included in this work. Further, the pulser was included to check wether the throughput of the system was affected by the shape of the puler peaks or not.

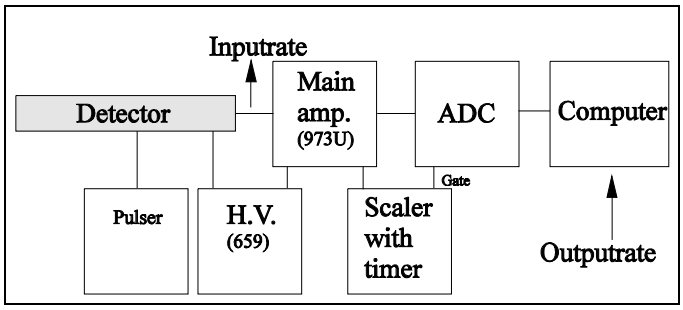

Figure 25. Set-up used to measure throughput of the system.

table 9 below shows the tabulated results from this measurement and figure 27 below shows the throughput in a graph form. Three pulse shapes, see figure 26, was used to investigate the functional dependence of the throughput curve. The frequency of the pulser was 1007±1 Hz.

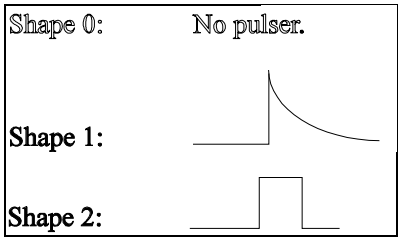

Figure 26. Different pulse shapes used in the throughput measurement.

The curve in figure 27 shows that the throughput is weakly dependent on the shape of the pulser peak. Shape 2 (square pulse) seem to have a slight degradation in throughput at relatively small counting rates. The significant difference in throughput comes from the integration time on the amplifier. Smaller integration time results in a higher throughput at larger counting rates but also in a worse energy resolution. The latter parameter has not been investigated in this work. The measurements indicate that the system is capable of handling counting rates up to 10^5 cps with a deadtime of the system not exceeding 50 %.

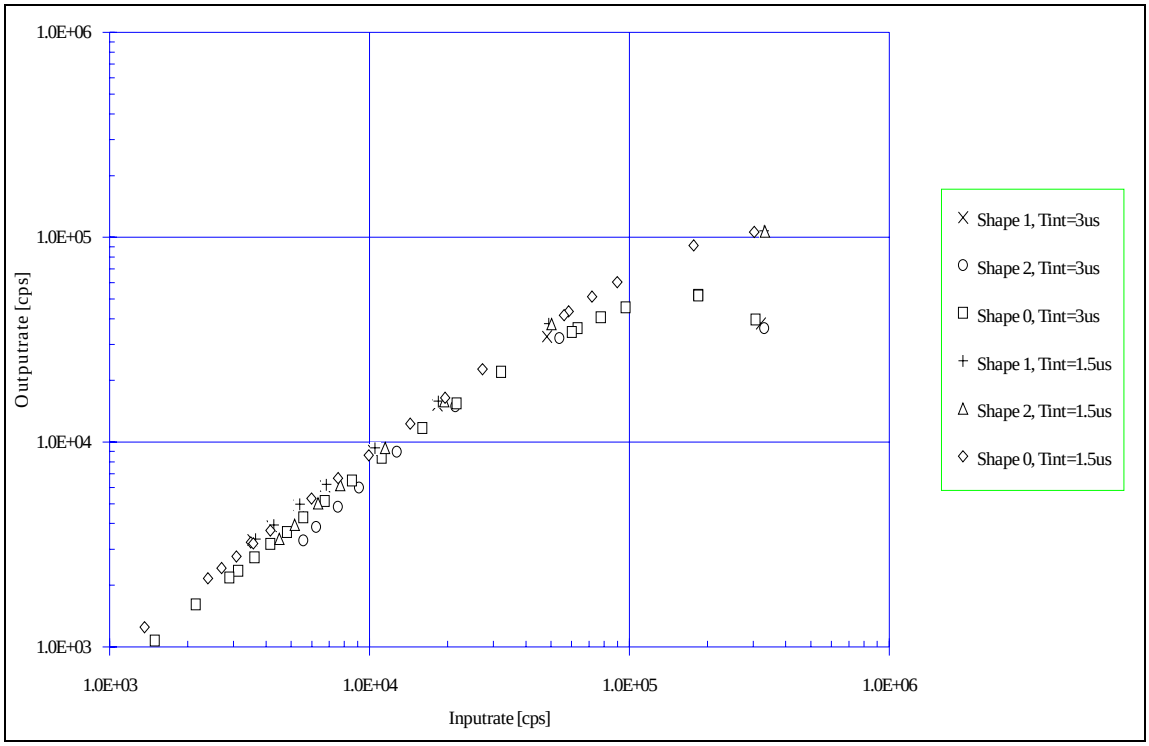

Figure 27. Graphical results from the throughput measurement.

File	Time	Counts	T(int.)	Pulse-	Sum (whole	Rate (whole	Rate
	(scaler) [ms]	(scaler)	[E-6 s]	shape	spectrum)	spectrum)	(scaler)
Co-60; files co601-co607, rest is Cs-137				(0,1 or 2)		[cps]	[cps]
co601	10000	14918	3.0	0		1070.4	1491.8
co602	10000	21520	3.0	0		1604.6	2152.0
co603	10000	321685	3.0	0		22045.5	32168.5
co609	10000	778585	3.0	0		40690.2	77858.5
co610	10000	1840292	3.0	0		52119.1	184029.2
co611	100000	18434793	3.0	0		52074.5	184347.9
co614	20000	1931644	3.0	0		45596.4	96582.2
co615	20000	1266143	3.0	0		35936.9	63307.2
co618	20000	434067	3.0	0		15415.3	21703.4
co619	20000	319563	3.0	0		11700.5	15978.2
co622	20000	222898	3.0	0		8361.6	11144.9
co623	20000	171458	3.0	0		6489.1	8572.9
co625	20000	134695	3.0	0		5135.4	6734.8
co627	20000	111326	3.0	0		4271.1	5566.3
co628	20000	96465	3.0	0		3635.5	4823.3
co630	20000	83182	3.0	0		3188.4	4159.1
co632	20000	72266	3.0	0		2734.7	3613.3
co634	20000	62614	3.0	0		2356.1	3130.7
co636	20000	57967	3.0	0		2174.1	2898.4
co638	20000	6112168	3.0	0		39541.7	305608.4
co640	20000	1206097	3.0	0		34529.6	60304.9
co604	10000	7531	1.5	0		698.3	753.1
co605	10000	13611	1.5	0		1252.4	1361.1
co606	10000	272096	1.5	0		22655.7	27209.6
co607	10000	35035	1.5	0		3239.9	3503.5
co608	10000	717841	1.5	0		51309.0	71784.1
co612	100000	17664730	1.5	0		90841.6	176647.3
co613	20000	1798403	1.5	0		60620.6	89920.2
co616	20000	1169522	1.5	0		43437.4	58476.1
co617	20000	392114	1.5	0		16422.6	19605.7
co620	20000	287343	1.5	0		12287.1	14367.2
co621	20000	198695	1.5	0		8651.2	9934.8
co624	20000	151613	1.5	0		6659.7	7580.7
co626	20000	119526	1.5	0		5297.3	5976.3
co629	20000	83264	1.5	0		3705.5	4163.2
co631	20000	71534	1.5	0		3207.8	3576.7
co633	20000	61553	1.5	0		2767.7	3077.7
co635	20000	53839	1.5	0		2425.6	2692.0
co637	20000	47809	1.5	0		2156.6	2390.5
co639	20000	6055360	1.5	0		106072.8	302768.0
co641	20000	1120729	1.5	0		41646.8	56036.5
cs1	40000	12819843	3.0	1	1514836	37880.2	320496.1
cs5	40000	1927768	3.0	1	1308964	32732.1	48194.2
cs9	20000	364310	3.0	1	302243	15115.8	18215.5
cs13	20000	206289	3.0	1	181211	9062.8	10314.5
cs17	20000	134788	3.0	1	121791	6091.0	6739.4
cs21	20000	106747	3.0	1	97961	4899.3	5337.4
cs25	20000	83829	3.0	1	77902	3896.1	4191.5
cs29	20000	70921	3.0	1	66431	3322.4	3546.1
cs3	40000	13204221	1.5	1	4298805	107496.4	330105.5
cs7	20000	979572	1.5	1	757925	37905.5	48978.6
cs11	20000	368030	1.5	1	317283	15868.0	18401.5
cs15	20000	209613	1.5	1	187083	9356.4	10480.7
cs19	20000	136695	1.5	1	123962	6199.6	6834.8
cs23	20000	108125	1.5	1	99301	4966.3	5406.3
cs27	20000	85625	1.5	1	78991	3950.5	4281.3
cs31	20000	72953	1.5	1	67171	3359.4	3647.7
cs2	40000	13251108	3.0	2	1434512	35871.6	331277.7
cs6	40000	2150276	3.0	2	1282003	32057.9	53756.9
cs10	20000	428222	3.0	2	297881	14987.7	21411.1
cs14	20000	254947	3.0	2	178772	8940.8	12747.4
cs18	20000	182117	3.0	2	119801	5991.5	9105.9
cs26	20000	124974	3.0	2	76961	3849.0	6248.7
cs22	20000	151314	3.0	2	96742	4838.3	7565.7
cs30	20000	111676	3.0	2	66111	3306.4	5583.8
cs4	40000	13287617	1.5	2	4276310	106933.9	332190.4
cs8	20000	1002616	1.5	2	753674	37692.9	50130.8
cs12	20000	388595	1.5	2	316291	15818.4	19429.8
cs16	20000	229729	1.5	2	187421	9373.3	11486.5
cs20	20000	154274	1.5	2	123361	6169.6	7713.7
cs24	20000	127052	1.5	2	100111	5006.8	6352.6
cs28	20000	103010	1.5	2	78641	3933.0	5150.5
cs32	20000	89919	1.5	2	67141	3357.9	4496.0

Table 9. Results of the throughput measurement.

6.2 TheFAT, Simulation of Gamma Radiation Leakage

6.2.1 Basic Geometric Assumptions and Simplifications

The geometry of a fuel assembly is shown in figure 28 and it is obvious that the spacers contribute to the attenuation only with a small fraction. Therefore the impact on the result from these are ignored, since they are thin compared to the rest of the fuel assembly. The activity in the fuel is considered to be homogenous.

Furthermore, the top and bottom of the assemblies are assumed to completely absorb the gamma radiation that strikes them.

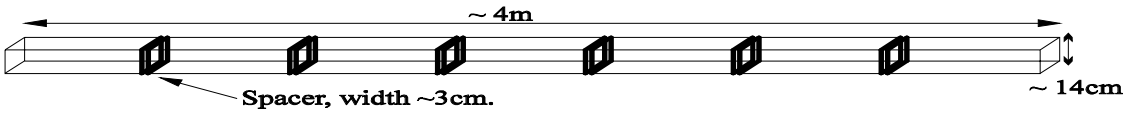

Figure 28. Geometry of a fuel assembly including the spacers.

With these assumptions the geometry essentially is symmetric in the z direction, (at least inside the assembly), and therefore it is only necessary to consider a grid in one plane. Knowing the attenuation in this plane, a simple integration can be performed in the θ direction to obtain the total attenuation or leakage fraction.

figure 29 shows some definitions made in order to integrate in the θ direction.

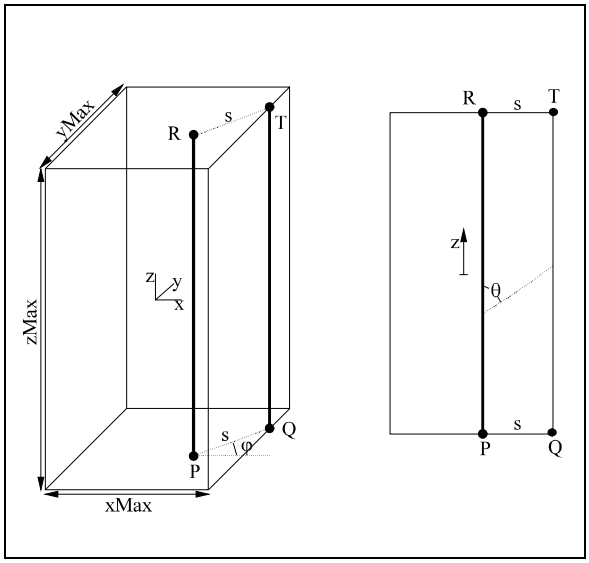

Figure 29. Definitions used in TheFAT in order to integrate in the z direction.

Assume that we know the value of the integral

$$I = -\int_P^Q \mu dl \,. \qquad \textit{Eq 17}$$

Here P and Q are the points shown in figure 29. This means that we know the attenuation, or leakage fraction, of a beam of gamma rays from P to Q.

The leakage fraction, F, is given by the expression

$$F = e^{I} = \exp\{ -\int_P^Q \mu dl \ \} \qquad \textit{Eq 18}$$

This expression comes from the familiar attenuation formula of gamma radiation through a bulk of material, $I=I_0 \cdot e^{-\mu x}$.

Since the assembly is considered to be symmetric in the z direction, it is straight forward to calculate the average leaking fraction.

$$\langle F \rangle = \int_0^{\pi} \int_{z_1}^{z_2} \frac{F}{\pi \cdot (z_1 - z_2)} dz d\theta = \frac{1}{\pi} \cdot \int_0^{\pi} F d\theta \qquad \textit{Eq 19}$$

This average is the average of the leaking fractions for all rays from the line PR to the line QT. See figure 29.

Here z_1 and z_2 are defined by the expressions

$$\begin{cases} 0 < \theta < \pi / 2: & \begin{cases} z_1 = zMax / 2 - s / \tan(\theta) \\ z_2 = -zMax / 2 \end{cases} \\ \pi / 2 < \theta < \pi: & \begin{cases} z_1 = zMax / 2 \\ z_2 = s / \tan(\pi - \theta) - zMax / 2 \end{cases} \end{cases} \qquad \textit{Eq 20}$$

The leakage fraction is dependent on θ since this angle defines the distance for the ray, see figure 29, in the medium and therefore the attenuation of the ray. Consequently the leakage fraction in the θ direction is written as

$$F = e^{I / \sin(\theta)} \qquad \textit{Eq 21}$$

and the average leakage fraction is written

$$\langle F \rangle = \frac{1}{\pi} \cdot \int_0^{\pi} e^{I / \sin\theta} d\theta = \frac{2}{\pi} \cdot \int_0^{\pi/2} e^{I / \sin\theta} d\theta \,. \qquad \textit{Eq 22}$$

The integral over θ is solved, using a numeric integration in the simulation program.

The main task of the program is to calculate a numeric value for the integral I. This is done by a 'ray-tracing' algorithm using the grid that is developed in the xy-plane. When the value of I is at hand, the only remaining task is to do the numeric integration over θ. This is described further below.

After each radiating grid point have been traversed, an average of the <F> values is calculated and the complete escape fraction is determined. Here, the activity is assumed to be constant within the fuel rods.

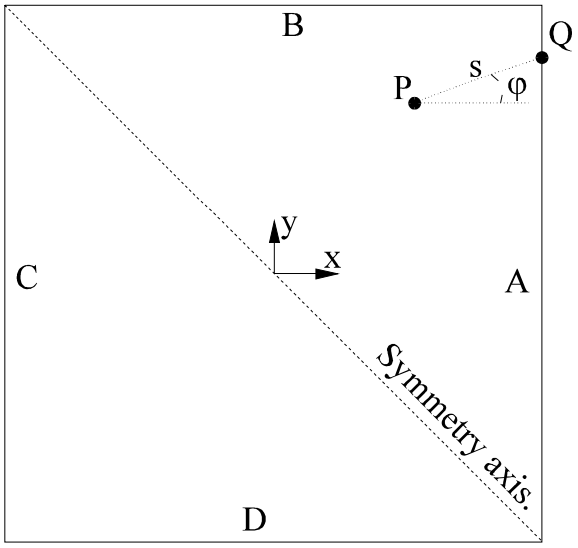

Figure 30. Symmetry of the assembly with the calorimeter. l_{PQ} is a line between P and Q with the equation $y-y_P=k\cdot(x-x_P)$ where $k=\tan(\varphi)$

One of the fuel rods in the middle of the fuel assembly is usually replaced by a channel of water. Therefore, the xy plane of the fuel assembly is symmetric in the diagonal of the plane. This symmetry is utilised in the simulation code. To calculate the integral of eq 17 only half of the grid needs to be traversed because of the symmetry. This is shown in figure 30.

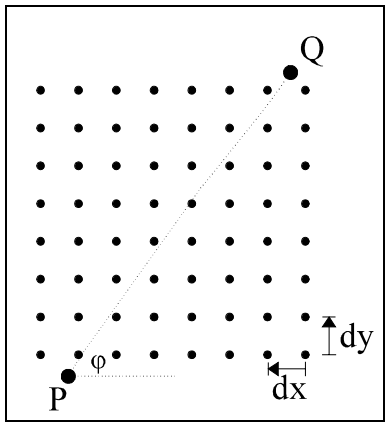

Figure 31. Part of the grid to illustrate the ray-tracing between the points P and Q.

Furthermore, it is necessary to divide the line l_{PQ} in figure 29 into discrete points in order to calculate the integral of eq 17. This is so, since the numerical calculation of this integral is a simple trapezoidal method of summing functional values.

figure 31 shows a part of the grid that is used in the program. In the program the variable n is defined as the number of parts that the line PQ is divided into.

The variable dr is defined as $dr=\sqrt{(dx)^2+(dy)^2}$. This is the unit of length used when tracing the ray towards the point Q. This means that $n=\left\lfloor \frac{s}{dr} \right\rfloor$, the highest integer that is lower than or equal to s/dr.

To calculate n, it is necessary to know where the line l_{PQ} crosses the side of the calorimeter. The crossing point with one of the sides A,B,C,D of the calorimeter is (x_{Qi},y_{Qi}) where i=A,B,C or D. For instance, if $-\pi/2 \le \varphi \le \pi/2$ and $-yMax/2 \le y_{QA} \le yMax/2$, then line A is crossed by the line l_{PQ} at y_{QA} and thus, $x_Q=x_{QA}=xMax/2$ and $y_Q=y_{QA}= k\cdot x_{QA}+m$.

Again, the distance s is divided into n parts. These parts are used to traverse along the ray when calculating the integral I and the escape fraction F. The n+1 points along the line PQ are then given the coordinates

$$\begin{cases} x_0 = x_P \\ x_1 = x_0 + dx\_ray \\ \vdots \\ x_{n-1} = x_0 + (n-1)\cdot dx\_ray \\ x_n = x_0 + n\cdot dx\_ray \end{cases} \quad \begin{cases} y_0 = y_P \\ y_1 = y_0 + dy\_ray \\ \vdots \\ y_{n-1} = y_0 + (n-1)\cdot dy\_ray \\ y_n = y_0 + n\cdot dy\_ray \end{cases} \quad \text{where} \quad \begin{cases} dx\_ray = dr\cdot\cos\varphi \\ dy\_ray = dr\cdot\sin\varphi \end{cases}$$

The integral I from eq 17 is finally approximated by the sum

$$I \approx -\sum_{k=1}^{n} \frac{\mu_k+\mu_{k-1}}{2}\cdot dr = \frac{-dr}{2}\cdot\left(\mu_0+\mu_1+\mu_1+\mu_2+\ldots+\mu_{n-2}+\mu_{n-1}+\mu_{n-1}+\mu_n\right) = -dr\cdot\left(\sum_{k=0}^{n}\mu_k - \frac{\mu_0+\mu_n}{2}\right) \qquad \textit{Eq 23}$$

Where $\mu_i=\mu(NINT(x_i),NINT(y_i))$ and NINT(x) is the integer closest to x. Note that an average of two adjacent μ values is made at each point.

6.2.2 Input and Output to/from TheFAT

TheFAT input is supplied directly into the source code. This means that the program needs to be recompilated for every change in the input parameter set. This is justified by the fact that the input parameters are few and that the compilation only takes about half a minute. Of course this could easily be changed if the program needs to be developed. Parameters supplied as input are the number of grid points in the grid, the number of angles that is to be used at each radiating grid point, the width of the fuel assembly (xMax and yMax) including the calorimeter and the number of integration points in the numeric integration of eq 22. Also supplied as input is the energy interval used in the actual simulation.

The output from TheFAT is written to a text file. The file names are specified inside the code but this can also be easily changed. The output consists of the input parameters, the escape fraction together with the maximum and minimum value of the discrete sum (eq 23) for each energy in the specified interval and, finally, the number of radiating grid points. There is also a printout of the local time when the simulation

began and ended on the text file. Below is an example of the printout from TheFAT, using a grid of 300x300 in the xy-plane and 360 angles in the φ direction. The results from this printout are the ones used in the leakage estimate for the gamma radiation from fuel of the BWR type with 8×8 fuel rods and one rod replaced with water (see appendix 6.2.5).

```
######################################################################
                1995-10-30; 08:37:10,375
######################################################################
xMax:  1.7700E-01    yMax:  1.7700E-01       xyGrid:  300
Number of angles:  360
----------------------------------------------------------------------
   Energy [MeV]       Fraction [%]      min(I)       max(I)
----------------------------------------------------------------------
    3.000E-02       5.20194020E-42   8.9496E+01   3.3543E+03
    4.000E-02       5.50336106E-21   4.1821E+01   1.6241E+03
    5.000E-02       1.19704669E-12   2.3547E+01   9.1030E+02
    6.000E-02       2.25720049E-08   1.4562E+01   5.6875E+02
    7.000E-02       4.50178385E-06   9.9232E+00   3.9210E+02
    8.000E-02       1.19009728E-04   7.1548E+00   2.7805E+02
    9.000E-02       9.31906869E-04   5.4972E+00   2.0803E+02
    1.000E-01       4.02568378E-03   4.3803E+00   1.5971E+02
    2.000E-01       7.70131582E-02   2.3603E+00   1.0471E+02
    3.000E-01       5.82675392E-01   1.2616E+00   4.3293E+01
    4.000E-01       1.47768908E+00   9.1560E-01   2.4827E+01
    5.000E-01       2.56264840E+00   7.4552E-01   1.7430E+01
    6.000E-01       3.69783078E+00   6.4087E-01   1.3677E+01
    7.000E-01       4.79600816E+00   5.8077E-01   1.1201E+01
    8.000E-01       5.75249409E+00   5.3825E-01   9.7587E+00
    9.000E-01       6.91880347E+00   4.8834E-01   8.6158E+00
    1.000E+00       8.09951984E+00   4.4730E-01   7.7189E+00
    1.250E+00       1.00891697E+01   4.0052E-01   6.4489E+00
    1.500E+00       1.17448366E+01   3.6696E-01   5.6985E+00
    1.750E+00       1.30290960E+01   3.4095E-01   5.2774E+00
    2.000E+00       1.41681069E+01   3.2113E-01   4.9370E+00
    2.250E+00       1.49303426E+01   3.0805E-01   4.7495E+00
    2.500E+00       1.55752619E+01   2.9804E-01   4.5929E+00
    2.750E+00       1.61989021E+01   2.8816E-01   4.4608E+00
    3.000E+00       1.69325492E+01   2.7840E-01   4.2964E+00
######################################################################
                1995-11-01; 04:42:32,618
######################################################################
```

Figure 32. Example of a printout from TheFAT. This printout was used in the calculations in appendix 6.2.5.

In table 10, is the results from the simulation with the program TheFAT, the escape fractions are shown for different energies. The first column specifies the gamma-ray energy and the remaining columns specifies the grid size.

E [MeV]	400x45	600x45	200x90	500x90	300x120	450x120	300x300	300x360
0.02			0.00					
0.03			0.00	0.00	0.00	0.00	0.00	0.00
0.04	0.00	0.00	0.00	0.00	0.00	0.00	0.00	0.00
0.05	0.00	0.00	0.00	0.00	0.00	0.00	0.00	0.00
0.06	0.00	0.00	0.00	0.00	0.00	0.00	0.00	0.00
0.07	0.00	0.00	0.00	0.00	0.00	0.00	0.00	0.00
0.08	0.00	0.00	0.00	0.00	0.00	0.00	0.00	0.00
0.09	0.00	0.00	0.00	0.00	0.00	0.00	0.00	0.00
0.1	0.01	0.01	0.00	0.01	0.00	0.01	0.00	0.00
0.2	0.10	0.15	0.04	0.12	0.08	0.11	0.08	0.08
0.3	0.65	0.77	0.48	0.59	0.58	0.67	0.59	0.58
0.4	1.55	1.73	1.35	1.36	1.48	1.57	1.48	1.48
0.5	2.63	2.87	2.44	2.29	2.57	2.65	2.57	2.56
0.6	3.77	4.04	3.58	3.26	3.70	3.78	3.70	3.70
0.7	4.86	5.16	4.71	4.24	4.80	4.86	4.80	4.80
0.8	5.81	6.14	5.69	5.10	5.76	5.81	5.76	5.75
0.9	6.97	7.33	6.87	6.11	6.92	6.97	6.92	6.92
1	8.16	8.54	8.06	7.13	8.10	8.15	8.10	8.10
1.25	10.14	10.56	10.10	9.00	10.09	10.12	10.09	10.09
1.5	11.79	12.24	11.78	10.54	11.75	11.77	11.75	11.74
1.75	13.08	13.54	13.08	11.72	13.03	13.05	13.03	13.03
2	14.22	14.70	14.22	12.74	14.17	14.19	14.17	14.17
2.25	14.98	15.47	14.99	13.47	14.93	14.95	14.93	14.93
2.5	15.63	16.13	15.64	14.07	15.58	15.60	15.58	15.58
2.75	16.26	16.76	16.26	14.65	16.20	16.22	16.20	16.20
3	16.99	17.50	17.00	15.36	16.93	16.95	16.94	16.93

Table 10. Results from the simulation with the program TheFAT. Specification NxM means that the grid had NxN grid points and M angles was used at every radiating grid point. The figures shows the percentage of the gamma radiation that escapes both the fuel assembly and the calorimeter.

6.2.3 The Source Code of the Program TheFAT

Below is the source code of the program TheFAT shown.

```
program TheFAT
implicit none
!#####################################################################
!       Please specify the following parameters.
!---------------------------------------------------------------------
  integer,parameter::xyGrid=500
  integer,parameter::num_of_angles=90
  integer,parameter::E_step_start=12
  integer,parameter::E_step_stop=36
  integer,parameter::num_of_integration_points=100
  integer,parameter::dp=KIND(0d0)
  real(kind=dp),parameter::xMax=0.177
  real(kind=dp),parameter::yMax=0.177
  real(kind=dp),parameter::t=1.6E-2, rFuel=0.522E-2, rZirc=0.6125E-2
!#####################################################################
character(len=12),dimension(1:3)::clock
integer,dimension(1:8)::date_time
real(kind=dp),dimension(1:8),parameter::RElem=t*(/-3.5,-2.5,-1.5, &
            -0.5,0.5,1.5,2.5,3.5/)
real(kind=dp)::x,y,pi
real(kind=dp),dimension(1:36)::Energies,myH2O,myU,myUO2,mySteel
real(kind=dp)::xMax_by_two,yMax_by_two,absx,absy
integer::i,j,n,l,E_step,ii,jj,fi,num_of_rad_lines
real(kind=dp),dimension(1:8,1:8)::r
real(kind=dp)::dx,dy,dr,J_integral,I_integral,min_I,max_I
real(kind=dp),dimension(:),allocatable::dx_ray,dy_ray
real(kind=dp),dimension(:),allocatable::yQA,xQB,yQC,xQD
real(kind=dp),dimension(:),allocatable::xQ,yQ
real(kind=dp),dimension(:),allocatable::k,m,exp_vek
real(kind=dp),dimension(:,:),allocatable::my
logical,dimension(:,:),allocatable::is_H2O,is_UO2,is_Steel
integer,dimension(:,:,:),allocatable::n_matrix
real(kind=dp),dimension(:),allocatable::my_vek
integer,dimension(:),allocatable::i_vek,j_vek,n_vek
real(kind=dp),dimension(:),allocatable::phi,sin_vek ! k=tan(phi)
!---------------------------------------------------------------------
call DATE_AND_TIME(clock(1),clock(2),clock(3),date_time)
call print_date_and_time
!---------------------------------------------------------------------
! my(H2O) and my(U) from reference [10].
! Accuracy: <5% below 5keV, 2% between 5keV and 10MeV
! my(Steel 8-18) from reference [12].
! Accuracy: ~10% (Approximation)
! Densities from reference [13].
! my(Zircaloy) and my(Box material) is approximated by my(Steel).
!---------------------------------------------------------------------
Energies= &             !Unit=[MeV]
      (/0.001_dp,0.002_dp,0.003_dp,0.004_dp,0.005_dp,0.006_dp,0.007_dp,
&
      0.008_dp,0.009_dp,0.01_dp,0.02_dp,0.03_dp,0.04_dp,0.05_dp,0.06_dp,
&
      0.07_dp,0.08_dp,0.09_dp,0.1_dp,0.2_dp,0.3_dp,0.4_dp,0.5_dp,0.6_dp,
&
      0.7_dp,0.8_dp,0.9_dp,1.0_dp,1.25_dp,1.5_dp,1.75_dp,2.0_dp,2.25_dp ,
&
      2.5_dp,2.75_dp,3.0_dp/)
myH2O= &            !Unit=[1/m] Values in parathesis are d(1/2)*rho,
[g/cm2].
                    ! T=293K: rho(H2O)=0.997 g/cm3.
      100*LOG(2._dp)/( &
      (/1.65E-4_dp,1.25E-3_dp,3.60E-3_dp,8.5E-3_dp,1.65E-2_dp,2.85E-
2_dp, &
      4.5E-2_dp,6.75E-2_dp,9.5E-2_dp,1.35E-1_dp,8.75E-
1_dp,1.85_dp,2.6_dp, &
      3.1_dp,3.4_dp,3.65_dp,3.8_dp,4.0_dp,4.15_dp,5.0_dp,5.9_dp,6.5_dp,
&
      7.3_dp,7.75_dp,8.25_dp,8.75_dp,9.25_dp,9.75_dp,11.0_dp,12.0_dp, &
      13.1_dp,13.5_dp,14.8_dp,15.5_dp,16.5_dp,17.5_dp/)/0.997_dp)
myU= &              !Unit=[1/m] T=300K: rho(U)=18.9 g/cm3.
      100*LOG(2._dp)/( &
      (/9.5E-5_dp,3.1E-4_dp,9.25E-4_dp,6.25E-4_dp,8.5E-4_dp,1.05E-3_dp,
&
      1.65E-3_dp,2.25E-3_dp,3.1E-3_dp,3.9E-3_dp,1.00E-2_dp,1.70E-2_dp,
&
      3.5E-2_dp,6.25E-2_dp,1.0E-1_dp,1.45E-1_dp,2.05E-1_dp,2.75E-1_dp,
&
      3.6E-1_dp,5.4E-1_dp,1.35_dp,2.45_dp,3.6_dp,4.7_dp,5.9_dp,6.9_dp, &
      7.9_dp,8.9_dp,10.9_dp,12.5_dp,13.5_dp,14.5_dp,15.0_dp,15.5_dp, &
      15.9_dp,16.5_dp/)/18.9_dp)
myUO2=238.0_dp*10.47_dp/(238.0_dp+32.0_dp)*myU/18.9_dp
mySteel= &          !Unit=[1/m] 74%Fe, 18%Cr, 8%Ni.
      100*LOG(2._dp)/( &
      (/7.E-5_dp,4.4E-4_dp,1.3E-3_dp,2.8E-3_dp,5.1E-3_dp,6E-3_dp, &
      5.8E-3_dp,2.4E-3_dp,3.0E-3_dp, 3.8E-3_dp,0.027_dp,0.08_dp, &
      0.18_dp, 0.32_dp,0.53_dp,0.8_dp,1.1_dp,1.4_dp,1.7_dp, &
      4.6_dp,6.2_dp,7.1_dp,8.0_dp,9.0_dp,9.5_dp,10.0_dp,11.0_dp,12.0_dp,
&
      13.0_dp,14.0_dp,15.0_dp,16.0_dp,16.5_dp,17.0_dp, &
      17.5_dp,18.0_dp/)/7.8_dp)
!---------------------------------------------------------------------
pi=4.0_dp*atan(1.0_dp)
xMax_by_two=xMax/2; yMax_by_two=yMax/2
dx=xMax/(xyGrid+1); dy=yMax/(xyGrid+1); dr=sqrt(dx**2+dy**2)
!---------------------------------------------------------------------
allocate(my(-xyGrid/2:xyGrid/2,-xyGrid/2:xyGrid/2))
allocate(is_H2O(-xyGrid/2:xyGrid/2,-xyGrid/2:xyGrid/2))
allocate(is_UO2(-xyGrid/2:xyGrid/2,-xyGrid/2:xyGrid/2))
allocate(is_Steel(-xyGrid/2:xyGrid/2,-xyGrid/2:xyGrid/2))
allocate(n_matrix(-xyGrid/2:xyGrid/2,-
xyGrid/2:xyGrid/2,1:num_of_angles))
allocate(dx_ray(1:num_of_angles),dy_ray(1:num_of_angles), &
            exp_vek(0:num_of_integration_points))
allocate(yQA(1:num_of_angles),xQB(1:num_of_angles), &
            yQC(1:num_of_angles),xQD(1:num_of_angles), &
            yQ(1:num_of_angles),xQ(1:num_of_angles), &
            k(1:num_of_angles),m(1:num_of_angles))
allocate(phi(1:num_of_angles),sin_vek(0:num_of_integration_points))
!---------------------------------------------------------------------
! Set physical parameters according to the geometry given.
!---------------------------------------------------------------------
sin_vek=sin((/(i*pi/(2*num_of_integration_points), &
            i=0,num_of_integration_points)/))
exp_vek=0.0_dp
where(abs(sin_vek)>1E-10)  exp_vek=exp(-dr/sin_vek)
deallocate(sin_vek)

phi=(/(i-1,i=1,num_of_angles)/)*2*pi/num_of_angles
where(phi==(pi/2))  k=9E10
where(phi==(3*pi/2))  k=-9E10
where(phi/=(pi/2) .and. phi/=(3*pi/2))    k=tan(phi)
dx_ray=dr*cos(phi); dy_ray=dr*sin(phi)
deallocate(phi)

call print_headline
!#####################################################################
is_H2O=.false.
is_UO2=.false.
is_Steel=.false.
num_of_rad_lines=0
do i=-xyGrid/2,xyGrid/2
      x=i*dx; absx=abs(x)
      do j=-i,xyGrid/2
            y=j*dy; absy=abs(y)
            do ii=1,8; do jj=1,8
                  r(ii,jj)=sqrt((x-RElem(ii))**2+(y-RElem(jj))**2)
            end do; end do
            if( (absx>=72.5E-3 .and. absx<=75.5E-3 .and. absy<=75.5E-3) &
            .or.(absx>=85.5E-3 .and. absx<=88.5E-3 .and. absy<=88.5E-3) &
            .or.(absy>=72.5E-3 .and. absy<=75.5E-3 .and. absx<=75.5E-3) &
            .or.(absy>=85.5E-3 .and. absy<=88.5E-3 .and. absx<=88.5E-3) &
                                    ) then
                  is_Steel(i,j)=.true.
            else if (any(r<=rFuel)) then
                  if (r(5,4)<=rFuel) then  ! Water channel.
                        is_H2O(i,j)=.true.
                  else
                        is_UO2(i,j)=.true.
                        num_of_rad_lines=num_of_rad_lines+1
                  end if
            else if (any(r<rZirc)) then
                  is_Steel(i,j)=.true.
            else if (absx<72.5E-3 .and. absy<72.5E-3) then
                  is_H2O(i,j)=.true.
            end if
            is_H2O(-j,-i)=is_H2O(i,j)  ! Mirror image in line y=-x.
            is_UO2(-j,-i)=is_UO2(i,j)
            is_Steel(-j,-i)=is_Steel(i,j)

            if (is_UO2(i,j)) then
                  m=y-k*x
                  yQA=k*xMax_by_two+m
                  yQC=m-k*xMax_by_two
                  where(k/=0)
                        xQB=(yMax_by_two-m)/k
                        xQD=(-yMax_by_two-m)/k
                  elsewhere
                        xQB=9E10
                        xQD=9E10
                  end where
                  where(abs(yQA)<=yMax_by_two .and. dx_ray>0)
                        xQ=xMax_by_two
```

```
                yQ=yQA
            end where
            where(abs(xQB)<=xMax_by_two .and. dy_ray>0)
                xQ=xQB
                yQ=yMax_by_two
            end where
            where(abs(yQC)<=yMax_by_two .and. dx_ray<0)
                xQ=-xMax_by_two
                yQ=yQC
            end where
            where(abs(xQD)<=xMax_by_two .and. dy_ray<0)
                xQ=xQD
                yQ=-yMax_by_two
            end where
            n_matrix(i,j,:)=floor(sqrt((xQ-x)**2+(yQ-y)**2)/dr)
        end if
    end do
end do
!###############################################################
!###############################################################
do E_step=E_step_start,E_step_stop

    my=0.0_dp
    where( is_H2O ) my=myH2O(E_step)
    where( is_UO2 ) my=myUO2(E_step)
    where( is_Steel ) my=mySteel(E_step)

!###############################################################
! Ray trace. (Calculate I at every grid point and the total integral J.)

    J_integral=0.0_dp
    I_integral=0.0_dp
    min_I=1E10; max_I=-1E10

    do i=-xyGrid/2,xyGrid/2
        x=i*dx
        do j=-i,xyGrid/2
            y=j*dy
            if (is_UO2(i,j)) then
                do fi=1,num_of_angles
                    n=n_matrix(i,j,fi)
                    allocate(n_vek(0:n),my_vek(0:n), &
                        i_vek(0:n),j_vek(0:n))
                    n_vek=(/(ii,ii=0,n)/)
                    my_vek=0.0_dp
                    i_vek=nint((x+n_vek*dx_ray(fi))/dx)
                    j_vek=nint((y+n_vek*dy_ray(fi))/dy)
                    do ii=0,n
                        if(abs(i_vek(ii))<=xyGrid &
                            .and. abs(j_vek(ii))<=xyGrid) &
                            my_vek(ii)=my(i_vek(ii),j_vek(ii))
                    end do

    I_integral=0.5_dp*(my_vek(0)+my_vek(n))+sum(my_vek)
                    if(I_integral>max_I) max_I=I_integral
                    if(I_integral<min_I) min_I=I_integral
                    J_integral=J_integral+sum(exp_vek**I_integral)
                    deallocate(n_vek,my_vek,i_vek,j_vek)
                end do
            end if
        end do
    end do
    if (num_of_rad_lines/=0) then
        J_integral=J_integral*100/((num_of_integration_points+1)* &
            num_of_rad_lines*num_of_angles)
    else
        J_integral=J_integral*100/((num_of_integration_points+1)* &
            num_of_angles)
    end if
    call print_results_for_this_energy
end do
!###############################################################
!###############################################################
call DATE_AND_TIME(clock(1),clock(2),clock(3),date_time)
call print_date_and_time
!---------------------------------------------------------------
contains
subroutine print_date_and_time
    open(unit=77,file="TheFAT.out",form="FORMATTED",position="AP
PEND")
    write(unit=77,fmt="(A)") " ############################ &
                              &#######################################"
    write(unit=77,fmt="(A,I4,A,I2.2,A,I2.2,A,I2.2,A,I2.2,A,I2.2,A,I3.3)") &
            "                ", &
            date_time(1),"-",date_time(2),"-", &
            date_time(3),"; ",date_time(5),":", &
            date_time(6),":",date_time(7),",",date_time(8)
    write(unit=77,fmt="(A)") " ############################ &

    &#######################################"
    close(unit=77)
end subroutine print_date_and_time
subroutine print_headline
    open(unit=77,file="TheFAT.out",form="FORMATTED",position="AP
PEND")
    write(unit=77,fmt="(A,ES11.4,A,ES11.4,A,I5)") " xMax:  ",xMax, &
                                  "   yMax: ",yMax,"      xyGrid: ",x yGrid
    write(unit=77,fmt="(A,I5)") " Number of angles: ",num_of_angles
    write(unit=77,fmt="(A)") " ----------------------------------------------------------
-----------"
    write(unit=77,fmt="(A)") "     Energy [MeV]      Fraction [%]   &
                                  &   min(I)      max(I)"
    write(unit=77,fmt="(A)") " ----------------------------------------------------------
-----------"
    close(unit=77)
end subroutine print_headline
subroutine print_results_for_this_energy
    open(unit=77,file="TheFAT.out",form="FORMATTED",position="AP
PEND")
    write(unit=77,fmt="(ES16.3,A,ES15.8,A,ES11.4,A,ES11.4)") &
            Energies(E_step),"              ",J_integral,"      ",min_I*dr,"
",max_I*dr
    close(unit=77)
end subroutine print_results_for_this_energy
end program TheFAT
```

6.2.4 Simple Case to Test the Code

It is easy to test if the minimum and maximum values of the integral I, (eq 17), in the output from TheFAT are correct. The calculation of these values is a straight forward procedure. See the different parameters in figure 33.

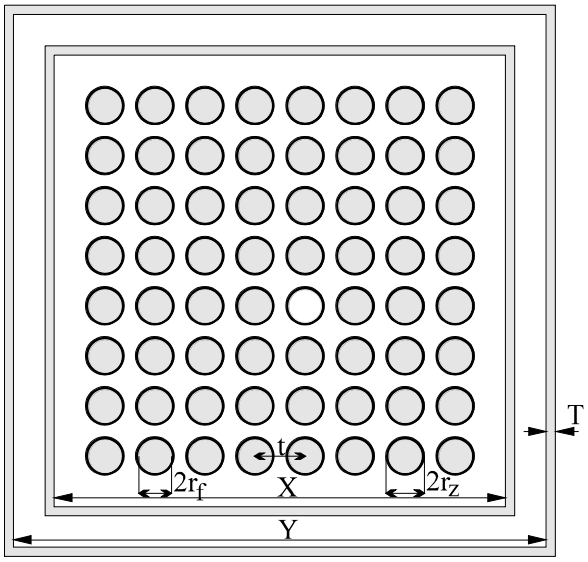

Figure 33. Geometric of a fuel assembly inside the calorimeter.

The numerical values of the parameters in figure 33 are

X=145mm
Y=171mm
T=3mm
r_f=5.22mm
r_z=6.125mm
t=16mm

When the energy of the gamma radiation is 1.0 MeV and the wall of the calorimeter is included in the calculation the values of I_{min} and I_{max} are

$I_{min}=\mu_{Steel}\cdot(t_{zirc.} + 2\cdot T)+\mu_{H2O}\cdot(X-8\cdot r_{zirc.}) / 2\approx 0.38$

(From the outer edge of a fuel rod perpendicular outwards to the outer wall of the calorimeter.)

$I_{max}=16\cdot r_f\cdot\mu_{UO2}+15\cdot t_{zirc.}\cdot\mu_{zirc.}+2\cdot\sqrt{2}\cdot T\cdot\mu_{steel}+\mu_{H2O}\cdot t_{H2O}\approx 7.9$, where $t_{zirc.} = r_z - r_f$

(From the outer edge of the fuel rod in the lower left corner diagonal across the assembly to the outer wall of the calorimeter.)

These should be compared to the output in appendix 6.2.2. The simulated values are 0.45 and 7.7 respectively at a gamma energy of 1.0 MeV. Note that these I-values is defined in only one plane of the fuel assembly. It is seen that the code generates approximately correct results but the geometry of the fuel assemblies makes it difficult to judge the uncertainty of the output from the code. It is seen that the simulated value of I_{min} differs relatively more to the calculated value than I_{max}. This is explained by the constuction of the simulation code. The value of I_{min} is more sensitive to the number of points in the grid since its calculation involves a much smaller number of points than the calculation of I_{max}.

To test the code a case was constructed where the geometry was highly simplified. figure 34 show a drawing of the geometry chosen for this test. The program TheFAT was modified

slightly to conform with the geometry of figure 34. Below are the outputs from the executions of TheFAT. The grid in these executions had 500x500 grid points and 120 angles were used at each radiating point in the grid.

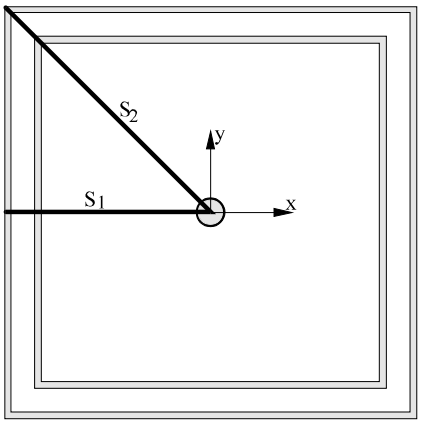

Figure 34. Geometry of the test example. One fuel rod in the centre and the walls of the calorimeter is included.

The first execution is with the walls of the calorimeter included (xMax=0.177 m) and the second is without the walls (xMax=0.145 m).

```
######################################################################
            1995-11-06; 11:24:00,766
######################################################################
xMax:  1.7700E-01    yMax:  1.7700E-01       xyGrid:  500
Number of angles:  120
----------------------------------------------------------------------
  Energy [MeV]       Fraction [%]      min(I)      max(I)
----------------------------------------------------------------------
   3.000E-02      9.75671246E-34   6.9552E+01   4.7481E+02
   4.000E-02      7.70768124E-17   3.2749E+01   2.2924E+02
   5.000E-02      3.69645721E-10   1.8882E+01   1.2899E+02
   6.000E-02      1.05500612E-06   1.2027E+01   8.0839E+01
   7.000E-02      7.98616818E-05   8.4666E+00   5.5921E+01
   8.000E-02      1.12330698E-03   6.3894E+00   4.0013E+01
   9.000E-02      6.11073560E-03   5.1276E+00   3.0252E+01
   1.000E-01      2.04163826E-02   4.2823E+00   2.3634E+01
   2.000E-01      2.89388461E-01   2.4954E+00   1.5212E+01
   3.000E-01      1.69364463E+00   1.6462E+00   7.0258E+00
   4.000E-01      3.87815589E+00   1.3503E+00   4.5339E+00
   5.000E-01      6.38664333E+00   1.1600E+00   3.4464E+00
   6.000E-01      8.60252571E+00   1.0486E+00   2.8772E+00
   7.000E-01      1.05864927E+01   9.7326E-01   2.4985E+00
   8.000E-01      1.22697885E+01   9.1285E-01   2.2572E+00
   9.000E-01      1.41907838E+01   8.4702E-01   2.0446E+00
   1.000E+00      1.60394505E+01   7.9082E-01   1.8720E+00
   1.250E+00      1.92280243E+01   7.0670E-01   1.6207E+00
   1.500E+00      2.17163114E+01   6.4869E-01   1.4620E+00
   1.750E+00      2.38683026E+01   5.9843E-01   1.3509E+00
   2.000E+00      2.52693337E+01   5.7250E-01   1.2799E+00
   2.250E+00      2.69323308E+01   5.3518E-01   1.2113E+00
   2.500E+00      2.80076897E+01   5.1439E-01   1.1672E+00
   2.750E+00      2.92329426E+01   4.9017E-01   1.1216E+00
   3.000E+00      3.04884958E+01   4.6800E-01   1.0749E+00
######################################################################
            1995-11-06; 11:45:56,793
######################################################################
```

```
######################################################################
            1995-11-06; 16:48:13,998
######################################################################
xMax:  1.4500E-01    yMax:  1.4500E-01       xyGrid:  500
Number of angles:  120
----------------------------------------------------------------------
  Energy [MeV]       Fraction [%]      min(I)      max(I)
----------------------------------------------------------------------
   3.000E-02      9.46019639E-15   2.8430E+01   4.1729E+02
   4.000E-02      8.27037755E-08   1.4273E+01   2.0327E+02
   5.000E-02      6.54459980E-05   8.5040E+00   1.1455E+02
   6.000E-02      1.92688328E-03   5.7386E+00   7.2181E+01
   7.000E-02      1.30154712E-02   4.2833E+00   5.0231E+01
   8.000E-02      4.76825612E-02   3.3639E+00   3.6003E+01
   9.000E-02      1.18467236E-01   2.7707E+00   2.7213E+01
   1.000E-01      2.36211198E-01   2.3628E+00   2.1140E+01
   2.000E-01      7.82926987E-01   1.7230E+00   1.4278E+01
   3.000E-01      3.44368183E+00   1.1296E+00   6.3402E+00
   4.000E-01      7.16886700E+00   9.2038E-01   3.9193E+00
   5.000E-01      1.10718003E+01   7.8578E-01   2.8952E+00
   6.000E-01      1.40959852E+01   7.1949E-01   2.3850E+00
   7.000E-01      1.69706458E+01   6.6415E-01   2.0301E+00
   8.000E-01      1.92856206E+01   6.2052E-01   1.8112E+00
   9.000E-01      2.15002202E+01   5.8203E-01   1.6387E+00
   1.000E+00      2.35647026E+01   5.4850E-01   1.4997E+00
   1.250E+00      2.76017423E+01   4.8377E-01   1.2762E+00
   1.500E+00      3.05233926E+01   4.4205E-01   1.1418E+00
   1.750E+00      3.29316211E+01   4.0551E-01   1.0520E+00
   2.000E+00      3.42461348E+01   3.9187E-01   9.9962E-01
   2.250E+00      3.62842138E+01   3.5972E-01   9.3949E-01
   2.500E+00      3.74756967E+01   3.4402E-01   9.0345E-01
   2.750E+00      3.88793756E+01   3.2449E-01   8.6540E-01
   3.000E+00      4.03186475E+01   3.0683E-01   8.2576E-01
######################################################################
            1995-11-06; 18:05:01,525
######################################################################
```

To compare these outputs with manual calculations a gamma-ray energy of 1.0 MeV was chosen. Furthermore, two paths (s_1 and s_2) were selected for two beams of gamma rays that represent the two extremes of minimum and maximum attenuation of the gamma rays. Two starting points for the gamma rays were also chosen. The first was given the distance r=<r>, from origin, and the second ray started from origin. Here <r> means the average value:

$$<r>=\int_0^{r_f} r\cdot e^{-\mu_{UO_2}\cdot r}dr \Big/ \int_0^{r_f} e^{-\mu_{UO_2}\cdot r}dr = \ldots = \frac{1}{\mu_{UO_2}} - \frac{r_f}{\exp\{\mu_{UO_2}\cdot r_f\}-1} \approx 2.45 \text{ mm}.$$

This value is a definition of the average value of r using a weight function that corresponds to the attenuation of gamma radiation through the material. table 11 below shows the distances the gamma rays passes through the various materials, also shown are the corresponding values of the integral I, (eq 19).

Material	Distance along s_1	⇒ Integral I, s_1	Distance along s_2	⇒ Integral I, s_2
Water	$X/2-r_f \approx 66.38$ mm	-0.47	$\sqrt{2}\cdot X/2-r_f \approx 96.41$ mm	-0.68
Fuel (from origin)	$r_f = 5.22$ mm	-0.38	$r_f = 5.22$ mm	-0.38
(from r=<r>)	$r_f-<r> \approx 2.77$ mm	-0.20	$r_f-<r> \approx 2.77$ mm	-0.20
Steel (with calorimeter)	$2\cdot T+r_z-r_f \approx 6.91$ mm	-0.31	$\sqrt{2}\cdot 2\cdot T+r_z-r_f \approx 9.39$ mm	-0.42
(without calorimeter)	$r_z-r_f \approx 0.91$ mm	-0.041	$r_z-r_f \approx 0.91$ mm	-0.041

Table 11. Distances that the four gamma rays used in the manual calculation passes through various materials. Also shown are the corresponding values of the integrals I, (eq 19). The different parameters used are shown in figure 33.

Using the values of table 11 and performing numerical calculations of the integral <F>, (eq 22), gives the average leakage fractions along s_1 and s_2. These are shown below, in table 12, together with the appropriate values from the outputs from the modified TheFAT executions.

	<F> along s_1	<F> along s_2	⇒ Average	Output from TheFAT
With calorimeter (from origin)	17.13 %	11.47 %	16.1 %	16.0 %
(from r=<r>)	21.42 %	14.23 %		
Without calorimeter (from origin)	24.21 %	18.42 %	24.1 %	23.6 %
(from r=<r>)	30.58 %	23.07 %		

Table 12. Calculated leakage fractions for the four gamma rays. The average shown is the average of these four rays. Compare with the output from TheFAT.

The manually calculated values are seen to be in reasonable agreement with the total escape fraction from TheFAT.

6.2.5 TheFAT Simulation Results for the Gamma-Scanned Fuel Assemblies

table 13 below shows the fraction of the total gamma radiation that remains inside the calorimeter with the assemblies used in this work according to simulations with TheFAT and gamma-scanning. These values are weighted averages of the non-escaping fractions for the visible peaks in the gamma ray spectrum from different fuel assemblies. The simulated values differ between different assemblies because of different gamma-ray spectra.

Assembly no.	Gamma-fraction escaping the box. [%]	Expected result from dosimetric measurement. [%]
8327	10.19 ± 1.53	9.38 ± 1.41
8332	10.14 ± 1.52	9.34 ± 1.40
8338	10.14 ± 1.52	9.34 ± 1.40
1136	10.06 ± 1.51	9.27 ± 1.39
582	10.05 ± 1.51	9.25 ± 1.39
596	10.06 ± 1.51	9.27 ± 1.39
710	10.06 ± 1.51	9.27 ± 1.39
900	10.07 ± 1.51	9.28 ± 1.39
6423	10.15 ± 1.52	9.35 ± 1.40
6454	10.15 ± 1.52	9.35 ± 1.40

Table 13. Results from the simulation with TheFAT and with the assemblies used here. The error is 15 % of the simulated escape fraction, which is also corrected by +15 % for the build-up.

To calculate these averages a curve on the form $f=a\cdot\exp\{-b/\sin(2\cdot E/\pi)\}$ was fitted to the diagram in figure 18 on page 31. This form of the functional behaviour of the escape fraction is based on the form of the integral in eq 22. Here a and b are the variable parameters and E is the gamma-ray energy, f is the escaping fraction. Also, the output shown in figure 32 was

used here, i.e. with a grid of 300x300 points in the xy-plane and 360 angles in the φ direction. Using the least square method gives the values 0.276 and 0.474 for a and b, respectively. This fitted curve was then used to calculate the weighted average using the twelve most significant peaks from the obtained spectra in the gamma scanning of the different fuel assemblies. The obtained spectra was corrected for efficiency before the averaging. Using the values supplied by ref. [10] on branching ratios for different isotopes it is possible to calculate the efficiency of the detector system and geometry.

$$\text{Efficiency}(E) = \frac{\textit{Known branching ratio }(E)}{\textit{Measured branching ratio }(E)} \qquad \textit{Eq 24}$$

The results from the gamma scanning of assemblies no. 6432 and 8327 and the values in ref. [10] was used to generate the diagram in figure 35 that shows the efficiency as a function of gamma radiation energy. This diagram was used as the efficiency correction mentioned above.

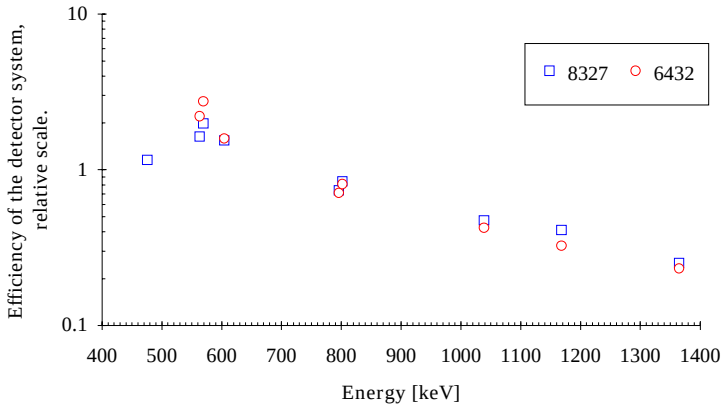

Figure 35. Energy dependence of the efficiency of the detector system used in the gamma scanning.

Using the simulated gamma-fractions, f, and the dosimetric/calorimetric measurement of the fraction f for assembly number 6432 (from section 5.2.1) it is possible to estimate the expected dosimetric results for the rest of the assemblies used in this work.

The gamma-fraction, $f_{6432}^{\text{measured}}$, for assembly number 6432 is given from section 5.2.3 as 9.3 ± 1.3 % and the simulated values for this assembly, $f_{6432}^{\text{simulated}}$, is 10.1 ± 1.5 %. Here, the effect of build-up is 15 % as discussed in section 5.2.2. A theoretical calculation of the expected dosimetric escape fraction for assembly number i, $f_{\text{i}}^{\text{expected}}$, is given by the expression

$$f_{\mathrm{i}}^{\mathrm{expected}} = f_{6432}^{\mathrm{measured}} \cdot \frac{f_{\mathrm{i}}^{\mathrm{simulated}}}{f_{6432}^{\mathrm{simulated}}} \qquad \textit{Eq 25}$$

table 13 summarises these calculated values for the assemblies used in this work.

6.3 Attenuation Coefficients

The linear attenuation coefficients of H_2O and of U are from reference [10] and the coefficients of steel are from reference [12]. For UO_2 the linear attenuation is calculated according to Bragg's law:

$$\frac{\mu_{UO_2}}{\rho_{UO_2}} = \frac{M_U}{M_U + M_{O_2}} \cdot \frac{\mu_U}{\rho_U} + \frac{M_{O_2}}{M_U + M_{O_2}} \cdot \frac{\mu_{O_2}}{\rho_{O_2}} \quad \Rightarrow \quad \mu_{UO_2} \approx \frac{M_U \cdot \rho_{UO_2}}{M_U + M_{O_2}} \cdot \frac{\mu_U}{\rho_U}$$

where $\begin{cases} \rho_i = \text{mass density of material i.} \\ M_i = \text{molecular weight of material i.} \\ \mu_i = \text{linear attenuation coefficient of material i.} \\ \mu_{O_2} \text{ is neglected in comparison with } \mu_U \end{cases}$ and $\begin{cases} M_U \approx 238 \\ M_{O_2} \approx 32 \\ \rho_{UO_2} \approx 10.47 g/cm^3 \\ \rho_U \approx 18.9 g/cm^3 \end{cases}$

from references [13] and [14].

E	my(H2O)	my(Steel)	my(U)	my(UO2)
[MeV]	[1/m]	[1/m]	[1/m]	[1/m]
0.001	4.19E+05	7.72E+06	1.38E+07	6.73E+06
0.002	5.53E+04	1.23E+06	4.23E+06	2.06E+06
0.003	1.92E+04	4.16E+05	1.42E+06	6.92E+05
0.004	8.13E+03	1.93E+05	2.10E+06	1.02E+06
0.005	4.19E+03	1.06E+05	1.54E+06	7.53E+05
0.006	2.42E+03	9.01E+04	1.25E+06	6.09E+05
0.007	1.54E+03	9.32E+04	7.94E+05	3.88E+05
0.008	1.02E+03	2.25E+05	5.82E+05	2.84E+05
0.009	7.27E+02	1.80E+05	4.23E+05	2.06E+05
0.01	5.12E+02	1.42E+05	3.36E+05	1.64E+05
0.02	7.90E+01	2.00E+04	1.31E+05	6.40E+04
0.03	3.74E+01	6.76E+03	7.71E+04	3.76E+04
0.04	2.66E+01	3.00E+03	3.74E+04	1.83E+04
0.05	2.23E+01	1.69E+03	2.10E+04	1.02E+04
0.06	2.03E+01	1.02E+03	1.31E+04	6.40E+03
0.07	1.89E+01	6.76E+02	9.03E+03	4.41E+03
0.08	1.82E+01	4.92E+02	6.39E+03	3.12E+03
0.09	1.73E+01	3.86E+02	4.76E+03	2.33E+03
0.10	1.67E+01	3.18E+02	3.64E+03	1.78E+03
0.20	1.38E+01	1.18E+02	2.43E+03	1.18E+03
0.30	1.17E+01	8.72E+01	9.70E+02	4.74E+02
0.40	1.06E+01	7.61E+01	5.35E+02	2.61E+02
0.50	9.47E+00	6.76E+01	3.64E+02	1.78E+02
0.60	8.92E+00	6.01E+01	2.79E+02	1.36E+02
0.70	8.38E+00	5.69E+01	2.22E+02	1.08E+02
0.80	7.90E+00	5.41E+01	1.90E+02	9.27E+01
0.90	7.47E+00	4.92E+01	1.66E+02	8.10E+01
1.00	7.09E+00	4.51E+01	1.47E+02	7.19E+01
1.25	6.28E+00	4.16E+01	1.20E+02	5.87E+01
1.50	5.76E+00	3.86E+01	1.05E+02	5.12E+01
1.75	5.28E+00	3.60E+01	9.70E+01	4.74E+01
2.00	5.12E+00	3.38E+01	9.03E+01	4.41E+01
2.25	4.67E+00	3.28E+01	8.73E+01	4.26E+01
2.50	4.46E+00	3.18E+01	8.45E+01	4.13E+01
2.75	4.19E+00	3.09E+01	8.24E+01	4.02E+01
3.00	3.95E+00	3.00E+01	7.94E+01	3.88E+01

Table 14. Linear attenuation coefficients used in TheFAT.

Below is table 14, the linear attenuation coefficients that was used in the execution of TheFAT. Linear interpolation between the points gives a linear attenuation coefficient for H_2O at 661.65 keV of 8.58 m^{-1}. Also from reference [10] is the coefficient for lead at 662 keV: 121 m^{-1}.

6.4 Results From Dosimetric Measurements

table 15 and table 16 below show the results from the initial dosimetric measurement and the measurement with several radial points, respectively. figure 36 shows a drawing of the container, (made of stainless steel), of the dosimetric probe that was used in the measurements. The container is filled with air that has negligible attenuation of the gamma radiation and the container is considered to have no influence on the results from the probe. See figure 14 on page 25 about the different coordinates and measurement points.

Assembly no.	Note	z[###] [m]	Dose rate [Sv / h]	Integral in z-direction.
			(+2.5 %- +7%)	
1136	In calorimeter.	0	0.65	63.22
	Distance from	1	16.2	
	top.	1.5	17.5	
		2	18.1	
		3	17.9	
		3.5	14.1	
		4	8	
1136	In calorimeter.	0	0.3	53.40
	Distance from	0.43	0.4	
	bottom.	1.16	15.3	
		1.46	15.7	
		1.86	16.7	
		2.31	17.1	
		3.45	11.6	
		3.93	10.8	
1136	Without calorimeter.	0.05	8.6	
	Distance from	0.3	20.3	
	bottom.	0.55	22.6	
	Start at 1:st side.	0.8	26.9	
		1.05	26.8	
		1.3	25.2	
		1.55	26.7	
		1.8	25.7	
		2.05	26.3	
		2.3	25.4	
		2.55	25.6	
		2.8	22.6	
		3.05	22	
		3.3	17.5	
		3.55	9.5	
		3.8	2.6	
	Corner of assembly.	1.8	20.1	
	2:nd side	3.8	2.6	
	(10cm from top)	3.55	9.8	
		3.3	19	
		3.05	24.6	
		2.8	24.6	
		2.55	28.3	
	Spacer ?	2.3	26.8	

[###] This measure of z is the distance from the top or the bottom of the assembly and is not the same as in figure 14.

		2.05	28.5	
		1.8	28.5	
		1.55	28.6	
		1.3	29.4	
		1.05	27.9	
		0.8	28.5	
	Spacer ?	0.55	24.9	
		0.3	21.6	
		0.05	8.5	
6432	In calorimeter.	0	1.5	134.06
	Distance from	1	38.6	
	top.	1.5	38	
		2	39.1	
		2.5	32.5	
		3	35.1	
		3.5	29	
		4	20.5	
6432	Without calorimeter.	Bottom	38	
	Distance from	0.5	64	
	bottom.	1	68	
		1.5	70.5	
		2	69.5	
		2.5	71	
		3	60	
		3.5	24	
		Top	3.7	

Table 15. Initial dosimetric measurement. Measurements at CLAB and data from reference [4].

Distance from top [cm] ↓	Distance from calorimeter to probe [cm] →	0	5	10	15	0	3	7	9	11	13	15
0		1.3	0.8	0.5		1.3	1					
70		32.5	19.6	11.8	7.6	29.2	23.1	16.1	12.6	10.5	8.6	7.4
104		40.4	23.2	13.6		36.6	27.2					
154		41.3	24.1	14.1		38.8	27.9					
181		40.6	24	14		39.5	28.7					
201		39.2	22.1	13.1	8.7	38.4	28.1	19.4	15.2	12.5	10.2	8.5
221		40.1	23.6	13.9		39.8	29.2					
283		36.5	22.7	12.5		37.4	27.4					
308		36.5	21.4	12.5		38	27.7					
321		35.9	21	12.6		37	27.1					
356		29.6	17.7	10.2	6.5	30.6	21.6	14	11.6	9.6	8	6.7
374		23.5	14.3	7.7		23.3	16.2					
Integral in z-direction. →		132.16				131.34						

Table 16. Dosimetric measurement with several radial measurement points on assembly number 6432 in the calorimeter. The table shows the dose rates in Sv/h. Side 1 were measured 1995-12-07 and side 2 on 1995-12-08 at CLAB.

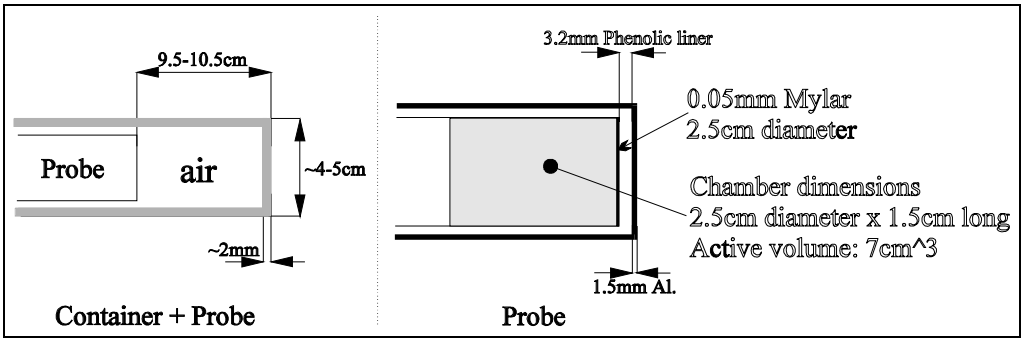

Figure 36. Dimemensions of the dosimetric probe and it's conatiner.

6.5 Results From the Gamma Scanning Experiment

The main results from the gamma scanning experiment are shown in table 17.

Assembly number	Cooling time [d]	Initial enrich-ment [%]	<Burnup> [Mwd/tU]	<Int ^{137}Cs>	<Int ^{134}Cs>	<Int ^{154}Eu>	<Int ^{137}Cs> Corrected	<Int ^{134}Cs> Corrected	<Int ^{154}Eu> Corrected
8327	1496	2.903	37842.16	1060.57	451.33	67.53	1072.17	528.82	70.15
8332	2595	2.895	34974.48	916.06	160.02	50.56	922.75	177.90	51.86
8338	2595	2.911	34823.08	887.01	157.45	49.83	893.49	175.05	51.11
1136	4473	2.491	22236.00	511.15	13.26	19.05	516.19	15.29	19.71
582	5552	2.255	21268.00	476.36	6.89	16.37	481.45	8.04	16.99
596	5552	2.255	22256.00	508.19	7.78	17.47	513.62	9.08	18.13
710	4803	2.258	22608.00	515.52	9.09	17.53	521.03	10.61	18.19
900	4803	2.258	23160.00	527.84	10.45	18.78	533.75	12.29	19.53
6423	2595	2.900	35105.52	938.33	199.60	56.35	947.34	229.39	58.26
6432	2595	2.894	36853.96	954.29	189.31	56.33	961.38	210.85	57.80
6454	3317	2.898	37234.64	940.80	128.11	54.94	944.31	135.26	55.66

Table 17. Tabulation of the different intensities from ^{137}Cs, ^{134}Cs and ^{154}Eu for the assemblies used in this work. Corrected intensity means that the measured intensity is multiplied with a factor that corrects the intensities with regards to the decay, (due to the time difference between cooling time at the gamma scanning and cooling time at the calorimetric measurement).

6.6 Results From Origen2.1 Simulations

table 18 shows the output from Origen2.1 that was used in figure 1 to figure 3**.** table 19 shows the values from the output of the Origen2.1 simulations for the eleven fuel assemblies used in this thesis. The calculations used one metric tonne of fuel and the values in table 19 are corrected for the actual weight[§§§] of the individual fuel assemblies.

Data for figure 1

CT [y]	Actinides	F. P.-Cs+Ba	137(Cs+Ba)	Act.-244Cm	244Cm
10.00	33.20	34.01	32.79	33.09	0.11
15.00	38.52	30.33	31.14	38.06	0.46
20.00	41.07	28.28	30.65	39.73	1.34
25.00	42.86	26.76	30.38	40.00	2.85
30.00	44.90	25.21	29.89	39.84	5.07
35.00	46.99	23.75	29.27	39.06	7.93
40.00	49.03	22.36	28.61	37.71	11.32
45.00	51.04	21.08	27.88	35.98	15.06

Data for figure 2

						Uncertainties			
CT [y]	Actinides	F.P.-(Cs+Ba)	137(Cs+Ba)	Act.-244Cm	244Cm	137(Cs+Ba)		244Am	
10.00	31.67	35.95	32.38	17.85	13.82	35.68	29.08	16.44	11.20
20.00	37.84	29.24	32.92	25.76	12.08	36.59	29.25		
30.00	42.43	26.25	31.32	32.56	9.87	35.12	27.52	11.27	8.47
40.00	46.99	23.74	29.27	39.06	7.93	33.16	25.38		
50.00	51.60	21.42	26.98	45.32	6.28	30.88	23.08	7.01	5.55

Data for figure 3

Initial enrichment [%]	137(Cs+Ba)	244Cm
1.00	27.67	15.79
2.00	29.36	7.98
3.00	31.09	3.61
4.00	32.90	1.54

Table 18. Contribution [%] to the decay heat from various sources in the spent fuel. F.P. and Act denotes fission products and actinides, respectively.

[§§§] As reported by SKB, ('Svensk Kärnbränslehantering AB'), data of fuel individes.

Nuclides ↓	Assembly number. ↓														
		Gamma-ray intensity													
		Cooling time													
		When the calorimetric measurement was performed.	1 [y]	2 [y]	6 [y]	8 [y]	10 [y]	13 [y]	15 [y]	16 [y]	18 [y]	20 [y]	25 [y]	37 [y]	50 [y]
^{137}Cs [Ci]	8327	18182	19318	18892		16440	15698		13986			12459	11101	8413	6230
	8332	15801	18054	17651		15364	14670		13071			11643	10374	7862	5823
	8338	15744	17990	17587		15311	14618		13023			11602	10336	7834	5802
	1136	8754	11242	10985			9132			7949	7589	7248	6457	4893	3624
	582	8534	11724	11456			9523			8290	7915	7557	6734	5102	3778
	596	8922	12257	11977			9955			8667	8275	7901	7040	5335	3950
	710	9101	11924	11651	10623				8628		8050	7686	6848	5190	3844
	900	9356	12252	11972	10915				8866		8272	7898	7036	5333	3950
	6423	16178	18445	18037		15696	14987		13352			11895	10598	8032	5948
	6432	16721	19119	18675		16257	15524		13831			12322	10976	8319	6160
	6454	16356	19634	19190			15952	14885	14213			12662	11279	8548	6331
^{134}Cs [Ci]	8327	5907	14281	10206		1357	693		129			24	4	0	0
	8332	2004	14044	10037		1335	681		127			24	4	0	0
	8338	1980	13877	9917		1319	673		125			23	4	0	0
	1136	172	6536	4670			317			42	22	11	2	0	0
	582	95	9632	6885			467			62	32	16	3	0	0
	596	103	10412	7442			505			67	34	18	3	0	0
	710	124	6289	4495	1171				57		21	11	2	0	0
	900	144	7300	5216	1359				66		24	12	2	0	0
	6423	2452	16611	11872		1579	806		150			28	5	0	0
	6432	2318	16211	11585		1541	787		146			27	5	0	0
	6454	1417	20309	14518			986	360	184			34	6	0	0
^{154}Eu [Ci]	8327	1688	2086	1925		1187	1010		675			451	301	115	40
	8332	1177	1876	1731		1067	908		607			406	271	103	36
	8338	1163	1854	1711		1055	898		600			401	268	102	36
	1136	354	846	781			410			253	215	183	122	46	16
	582	305	923	851			447			275	235	200	133	51	18
	596	333	1007	929			487			301	256	218	145	55	19
	710	359	921	850	616				298		234	199	133	51	18
	900	389	996	919	665				322		253	215	144	55	19
	6423	1237	1956	1805		1113	947		633			423	283	107	38
	6432	1304	2079	1917		1182	1006		672			449	300	114	40
	6454	1172	2219	2047			1074	843	718			480	321	122	43
Total [Ci]	8327	107172	197440	143606		78372	72264		61132			52716	45809	33256	23970
	8332	78907	210715	146187		74185	68203		57569			49617	43102	31279	22527
	8338	78586	208675	145114		73880	67948		57364			49443	42960	31186	22448
	1136	40922	156945	101542			43770			35723	33647	31725	27539	19972	14356
	582	39311	285959	160648			46903			37732	35461	33386	28897	20862	14938
	596	40898	296454	167028			48783			39267	36893	34731	30071	21707	15551
	710	41898	135818	95622	55799				38884		35497	33458	29043	21011	15096
	900	43205	159271	106364	58051				40031		36519	34426	29868	21603	15510
	6423	82276	257133	168407		76483	70032		58908			50716	44034	31933	22977
	6432	83612	231664	159200		78446	72038		60730			52315	45445	32965	23734
	6454	78216	312722	195807			74662	66862	62615			53856	46748	33884	24378
		Thermal heat													
		Cooling time													
		When the calorimetric measurement was performed.	1 [y]	2 [y]	6 [y]	8 [y]	10 [y]	13 [y]	15 [y]	16 [y]	18 [y]	20 [y]	25 [y]	37 [y]	50 [y]
^{137}Cs [W]	8327	20.12	21.38	20.90		18.18	17.36		15.47			13.78	12.28	9.30	6.89
	8332	17.48	19.97	19.53		17.00	16.23		14.46			12.88	11.47	8.70	6.44
	8338	17.42	19.91	19.45		16.93	16.17		14.40			12.83	11.43	8.66	6.42
	1136	9.68	12.43	12.15			10.10			8.79	8.40	8.02	7.14	5.41	4.01
	582	9.44	12.97	12.67			10.53			9.17	8.75	8.36	7.45	5.64	4.18
	596	9.87	13.56	13.25			11.01			9.59	9.15	8.74	7.79	5.90	4.37
	710	10.07	13.19	12.89	11.75				9.54		8.90	8.50	7.57	5.74	4.25
	900	10.35	13.55	13.24	12.07				9.81		9.15	8.74	7.78	5.90	4.37
	6423	17.89	20.42	19.94		17.36	16.58		14.77			13.16	11.72	8.88	6.58
	6432	18.50	21.14	20.66		17.98	17.17		15.30			13.63	12.14	9.20	6.81
	6454	18.09	21.73	21.23			17.65	16.46	15.72			14.00	12.48	9.46	7.00
^{137}Ba [W]	8327	67.56	71.79	70.15		61.06	58.31		51.95			46.27	41.23	31.25	23.14
	8332	58.69	67.08	65.56		57.07	54.50		48.55			43.24	38.54	29.20	21.62
	8338	58.48	66.85	65.32		56.87	54.31		48.38			43.10	38.40	29.09	21.54
	1136	32.51	41.76	40.80			33.92			29.53	28.19	26.92	23.99	18.17	13.46
	582	31.70	43.55	42.56			35.37			30.80	29.39	28.08	25.01	18.95	14.04
	596	33.14	45.52	44.49			36.98			32.20	30.74	29.34	26.15	19.81	14.67
	710	33.81	44.29	43.28	39.45				32.04		29.89	28.55	25.44	19.27	14.28
	900	34.75	45.51	44.46	40.54				32.94		30.72	29.34	26.14	19.81	14.67
	6423	60.10	68.54	66.98		58.30	55.67		49.60			44.19	39.36	29.84	22.09
	6432	62.11	70.99	69.37		60.39	57.66		51.37			45.76	40.78	30.91	22.88
	6454	60.75	72.96	71.29			59.26	55.29	52.79			47.03	41.90	31.75	23.51
^{134}Cs [W]	8327	60.14	145.35	103.87		13.82	7.05		1.31			0.24	0.05	0.00	0.00
	8332	20.40	142.92	102.14		13.59	6.94		1.29			0.24	0.04	0.00	0.00
	8338	20.16	141.22	100.93		13.42	6.85		1.28			0.24	0.04	0.00	0.00
	1136	1.75	66.50	47.53			3.23			0.43	0.22	0.11	0.02	0.00	0.00
	582	0.97	98.05	70.07			4.76			0.63	0.32	0.16	0.03	0.00	0.00

	596	1.04	105.98	75.73			5.14			0.68	0.35	0.18	0.03	0.00	0.00
	710	1.26	64.03	45.75	11.92				0.58		0.21	0.11	0.02	0.00	0.00
	900	1.47	74.30	53.10	13.83				0.67		0.24	0.13	0.02	0.00	0.00
	6423	24.95	169.06	120.84		16.07	8.20		1.53			0.28	0.05	0.00	0.00
	6432	23.59	164.99	117.91		15.68	8.01		1.49			0.28	0.05	0.00	0.00
	6454	14.42	206.82	147.76			10.03	3.66	1.87			0.35	0.06	0.00	0.00
^{154}Eu [W]	8327	15.10	18.66	17.22		10.61	9.03		6.04			4.04	2.70	1.03	0.36
	8332	10.52	16.78	15.48		9.55	8.13		5.43			3.63	2.42	0.92	0.32
	8338	10.40	16.59	15.31		9.44	8.03		5.37			3.59	2.40	0.91	0.32
	1136	3.16	7.57	6.98			3.66			2.26	1.92	1.64	1.09	0.42	0.15
	582	2.73	8.26	7.62			4.00			2.46	2.10	1.78	1.19	0.45	0.16
	596	2.98	9.01	8.31			4.36			2.69	2.29	1.95	1.30	0.49	0.17
	710	3.21	8.24	7.60	5.51				2.67		2.09	1.78	1.19	0.45	0.16
	900	3.48	8.91	8.22	5.95				2.88		2.26	1.93	1.29	0.49	0.17
	6423	11.06	17.50	16.15		9.95	8.47		5.66			3.78	2.53	0.96	0.34
	6432	11.66	18.59	17.15		10.57	9.00		6.01			4.02	2.69	1.02	0.36
	6454	10.48	19.85	18.30			9.61	7.54	6.42			4.29	2.87	1.09	0.38
Total [W]	8327	356.53	813.02	529.64		242.72	224.96		197.97			179.33	163.72	134.00	110.10
	8332	237.34	869.31	536.82		222.08	205.21		180.36			163.51	149.54	122.70	101.01
	8338	235.67	856.90	530.66		220.57	203.88		179.19			162.46	148.59	121.92	100.36
	1136	113.12	627.47	346.59			118.75			103.70	100.00	96.58	88.91	73.88	61.44
	582	107.84	1134.97	579.90			122.38			105.12	101.26	97.73	89.90	74.67	62.09
	596	113.09	1183.69	607.97			128.56			110.22	106.11	102.39	94.11	78.07	64.85
	710	116.51	500.72	308.69	148.64				111.15		105.20	101.63	93.60	77.87	64.88
	900	120.77	623.07	359.16	156.75				115.04		108.81	105.09	96.75	80.47	67.04
	6423	248.43	1082.73	636.35		228.70	209.86		183.21			165.71	151.38	123.98	101.86
	6432	257.23	969.61	598.77		239.83	220.83		193.50			174.91	159.71	130.69	107.33
	6454	239.69	1365.67	771.14			229.03	208.78	198.83			179.28	163.54	133.56	109.49

Table 19. Tabulation of the output from the simulations with Origen2. Here, the histories for assemblies no. 1136, 582, 596, 710 and 900 was incomplete with regards to accumulated burn-up in there first irradiation cycle. The burn-up values for cycle 1 was added to those in cycle 2.

7 References

[1] Anders Bäcklin, Ane Håkansson; ”Methods for fuel monitoring at the planned encapsulation plant”; Dept. of Radiation Sciences, Uppsala University; 1995-05-30

[2] Peter B.R. Björkholm, Anna T. Dyring; ”A STUDY OF A HIGH RATE GAMMA-SPECTROMETER SYSTEM FOR BURNUP MEASUREMENTS”; Thesis for the degree of MSc at the institute of technology; Uppsala University; January 1990; ISSN 0346-8887

[3] Ane Håkansson, Anders Bäcklin; ”NON-DESTRUCTIVE ASSAY OF SPENT BWR FUEL WITH HIGH-RESOLUTION GAMMA-RAY SPECTROSCOPY”; May 1995; ISSN 1104-1374; ISRN SKI-R--95/19--SE

[4] Agrenius Engineering AB, private communications.

[5] Drawing of the leak seeking equipment. Number 137483 at CLAB.

[6] Mark W. Zemansky, Richard H. Dittman; ”HEAT AND THERMODYNAMICS”; 6th edition; McGraw-Hill 1981; ISBN 0-07-066647-4

[7] Model RO-7; Ion Chamber technical Manual; Eberline, A division of Thermo Electron corporation; February 1983

[8] J. L. Parker; ”The Use of Calibration Standards and the Correction for Sample Self-Attenuation in Gamma-Ray Nondestructive Assay”; Los Alamos National Laboratory; LA-10045; August 1984

[9] JJ Fitzgerald, Brownwell & Mahoney; ”Mathematical Theory of Radiation Dosimetry”; Gordon-Breach 1967

[10] Lederer, Shirley; ”Table of Isotopes”; 7th edition; Wiley-Interscience 1978; ISBN 0-471-04179-3

[11] Glenn F. Knoll; ”RADIATION DETECTION AND MEASUREMENT”; 2nd edition; John Wiley & Sons,Inc; 1989

[12] PHILIPS; ”TRANSMISSION OF HIGH-ENERGY PHOTONS THROUGH VARIOUS MATERIALS”

[13] Carl Nordling, Jonny Österman; ”Physics Handbook”; Studentlitteratur 1987; ISBN 91-44-16574-9

[14] Suresh Garg, Feroz Ahmed, L.S. Kothari; ”PHYSICS OF NUCLEAR REACTORS”; Tata McGraw Hill 1986

[15] Documentation for CCC-371/ORIGEN 2.1 Code Package, N.E.A. Data Bank, August 1991

[16] SKB; World Wide Web page on the Internet 1996-04-29, http://www.lexivision.se/skb/pres/avfall/mycket.htm

[17] SKB; ”Verksamheten 1994”